A Facially Coordinating Tris-Benzimidazole Ligand for Nonheme Iron Enzyme Models: Biomimetic or Radical Aerobic Oxidation?

Parami S. Gunasekera,[†] Preshit C. Abhyankar,[†] Samantha N. MacMillan,[§] David C. Lacy*[†]

[†]*Department of Chemistry, University at Buffalo, State University of New York, Buffalo, New York 14260, United States.*
[§] *Department of Chemistry and Chemical Biology, Cornell University, Ithaca, New York 14853, United States.*

Supporting Information Placeholder

ABSTRACT: Herein, we report a rationally designed tripodal tris-benzimidazole ligand (**Tbim**) that structurally mimics the 3-His coordination environment of certain nonheme mono-nuclear iron oxygenases. The coordination chemistry of **Tbim** was explored with iron(II) and the ability of the iron complexes to oxidize biomimetic model substrates lithium diethyl 2-phenylmalonate and sodium thiocresolate was studied.

Molecular oxygen (O_2) is the most sustainable oxidant in oxidative transformation. It is no surprise then that the design of new catalysts take inspiration from (di)oxygenases, which are enzymes that incorporate O-atoms from O_2 into a substrate. Many of these enzymes are iron-dependent and contain a two-histidine one-carboxylate (2-His-1-C) facial triad binding pocket.[1,2] Recently, additional binding modes have been discovered, and these include the three-histidine (3-His), three-histidine one-carboxylate, and four histidine binding modes.[3]

Modelling the 3-His coordination has been attempted through various nitrogen donor ligands such as 1,4,7-triazacyclononane (**tacn**),[4] tris(2-pyridyl)methane (**Tpym**),[5] trispyrazolyl variants namely trispyrazolylborates (**Tp**),[6] trispyrazolylmethanes (**Tpm**)[7] and trisimidazolylphosphines (**TIP**),[8] and other ligands.[9,10] Some of these facially coordinating ligands have been used to prepare Fe-based O_2 derived oxidants, such as superoxo and oxo species,[11-16] and there are a few catalytic examples.[17,18]

In our pursuit to prepare structurally faithful 3-His mononuclear nonheme iron model complexes, we noted that despite similar coordination geometry, most of the ligands contain donor groups that are not representative of those in nature (Figure 1). For instance, histidine donors are imidazole nitrogen groups with sp^2 hybridization and in an aromatic ring. In contrast, **tacn** has sp^3 hybridization and is not conjugated. Accordingly, we noted that Gebbink and coworkers modeled the 2-His-1-C facial triad using imidazole and benzimidazole ligands

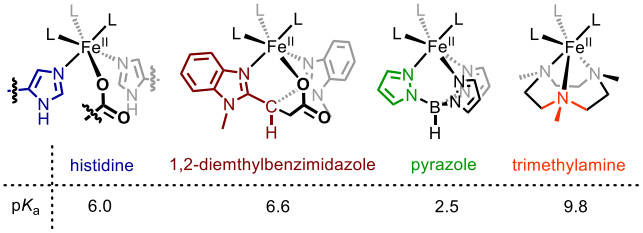

Figure 1. Natural two-histidine one-carboxylate enzyme binding site (left) compared to tridentate ligands with representative "mono-dentate" ligand donor groups and their respective $[NH]^+$ pK_a in water (see Fig. S19 and Table S1 for more examples).

(**2bim1C**) with surprising structural precision and also functional chemistry.[19,20] In addition to the electronic similarity (i.e. sp^2 hybridized and aromatized) with the donor groups in Gebbink's **2bim1C** and histidine, benzimidazole and imidazole have excellent pK_a similarities to histidine. For instance, the pK_a of the nitrogen donor of histidine is 6.0 in water,[21] which is close to the pK_a of 6.6 for 1,2-dimethylbenzimidazole that is the donor moiety in Gebbink's **2bim1C** ligand.[22,23] Ligands with similar coordination modes and electronic properties are thought to impart the appropriate thermodynamic requirements for functional chemistry.[24] Therefore, inspired by Gebbink's **2bim1C** ligand, we report herein the synthesis of a novel 3-His model with a tris-benzimidazole ligand, 2,2'-(2-(1-ethylbenzimidazol-2yl)ethane-1,1-diyl)bis(1-methylbenzimidazole) (**Tbim**), its coordination with iron and a brief foray into catalysis.

Synthesis. Our synthesis of the new ligand **Tbim** used a strategy similar to the one Gebbink used to prepare **2bim1C** (Scheme 1).[20,25,26] With ligand in hand, we explored the coordination chemistry of **Tbim** using a variety of FeX_2 salts (X = OAc, Cl, OTf). Inspired from certain successful work with **Tp*** to afford mono-ligated complexes,[11] we performed an analogous reaction with **Tbim** and $Fe(OAc)_2$ in a dichloromethane/acetonitrile solvent mixture (Scheme 2). Crystals suitable for diffraction revealed the mono-ligated complex [Fe{**Tbim**}$(OAc)_2$] (**1**) (Figure 2). Both acetates are κ-2 and **Tbim** is bound through the two benzimidazole arms

Scheme 1. Ligand Synthesis

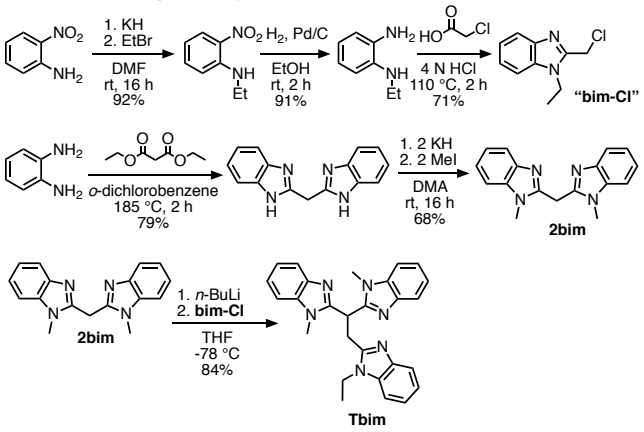

Scheme 2. Synthesis of 1 and 2

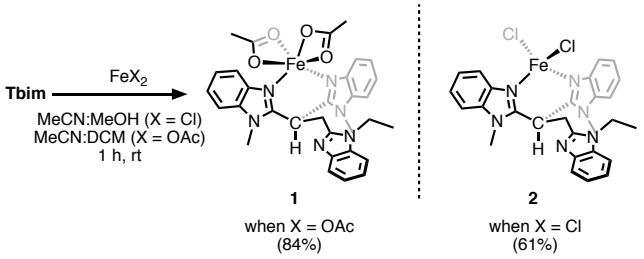

that form six-membered chelate rings. The third benzimidazole arm, if bound to the metal, would give a seven-membered ring that is apparently unfavored over acetate κ-2 coordination. The complex shows paramagnetically shifted ^{1}H NMR signals in the range −20 ppm to 90 ppm; Evans method was conducted and is consistent with an S = 2 ground state for **1** (μ_{eff} = 5.31). ATR-FTIR characterization shows C–O stretches from the acetate groups at 1605 and 1564 cm^{-1}. **Tbim** also reacts with $FeCl_2$ to produce the complex [Fe{**Tbim**}(Cl)$_2$] (**2**) that is structurally similar to **1** (Figure 2).

Salt metatheses were performed on **1** and **2** in an attempt to remove a single acetato or chlorido ligand and coordinate the third benzimidazole arm to iron. For instance, we attempted the reaction of **1** with $NaBPh_4$ in methanol. The reaction produced a yellow precipitate from which we obtained colourless crystals of the formulation [Fe{**Tbim**}$_2$][BPh_4]$_2$ ([**3**][BPh_4]$_2$), which is a bis-ligated metal complex salt whose connectivity was confirmed through XRD (Figure S16).

A reaction of **Tbim** with Fe(OTf)$_2$•2MeCN in acetonitrile also produced the bis-ligated metal complex [**3**][OTf]$_2$. However, if a different workup procedure was used for the same *in situ* prepared 1:1 ligand:metal mixture, a different product was obtained. Namely, if the acetonitrile reaction mixture was removed *in vacuo* to near dryness and the resulting residue dissolved in dichloromethane the mono-ligated metal complex [Fe{**Tbim**}(MeCN)$_2$(OTf)][OTf] ([**4**][OTf]) was obtained in moderate yields. The presence of acetonitrile ligands is confirmed from ATR-FTIR spectroscopy (ν_{CN} = 2279 and 2285 cm^{-1}) and X-ray crystallography

Scheme 3. Synthesis of [3]$^{2+}$ and [4]$^+$

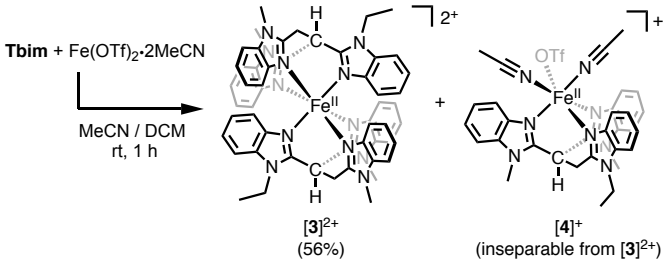

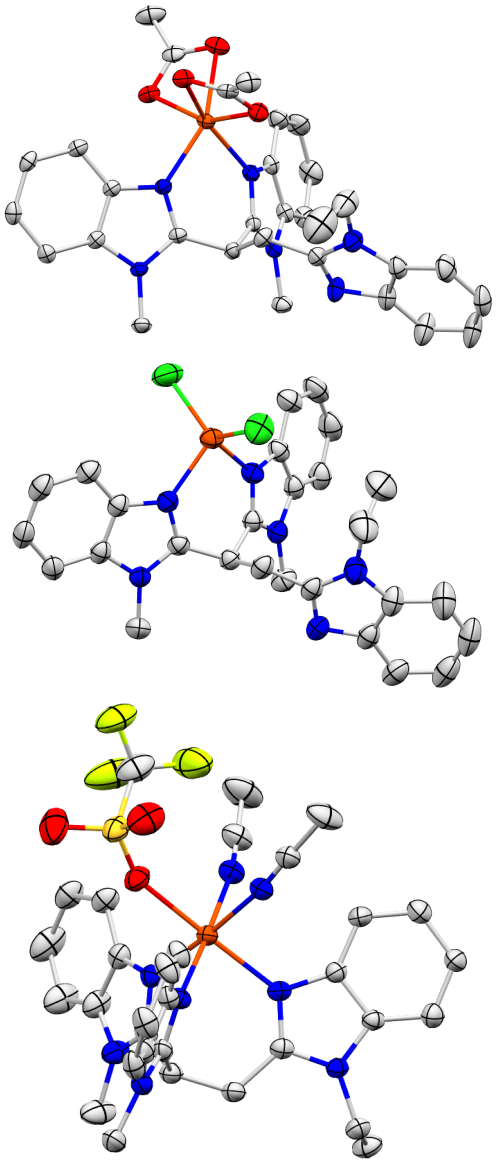

Figure 2. Molecular structure of (top to bottom) **1**,**2** and [**4**]$^+$ with ellipsoids shown at 50% probability; H-atoms, counterions, and solvent molecules are not shown. Color scheme: orange = Fe; blue = N; red = O; yellow/green = F; yellow = S; green = Cl; grey = C.

(Figure 2). Nevertheless, [**4**][OTf] was inseparable from [**3**][OTf]$_2$ under the conditions studied here.

Titration of **Tbim** with Fe(OTf)$_2$•2MeCN in acetonitrile followed by ^{1}H NMR and ^{19}F {^{1}H} NMR provided insight into the coordination behaviour of **Tbim** in

solution. The ^{1}H NMR data indicates the presence of both the mono-ligated and the bis-ligated complex in acetonitrile in a 1:1 reaction mixture (Figure S15). The ^{19}F {^{1}H} NMR spectrum of a 2:1 ligand:metal ratio contains a single, sharp peak at −80 ppm consistent with an unbound triflate ion for [**3**][OTF]$_2$.[20] In contrast, when the ratio is less than 2:1, a broad signal is apparent at −73 ppm indicative of an equilibrium between bound and unbound triflate ions in solution implicating the presence of mono-ligated species [**4**]$^+$ (Figure S12). This is consistent with a Schlenk equilibrium between [**3**]$^{2+}$ and [**4**]$^+$ at room temperature in MeCN; using density functional theory (DFT), the calculated equilibrium lies toward the bis ligated complex with a free energy of -3.2 kcal/mol (see SI). ^{1}H NMR spectroscopy was used to construct a kind of "Job plot" to determine the optimal ratio of Fe(OTf)$_2$:**Tbim** to prepare *in situ* [**4**]$^+$ for the catalysis studies later (Figure S17), and a Fe(OTf)$_2$:**Tbim** stoichiometry of 3:2 was the optimal ratio to achieve the highest concentration of [**4**]$^+$ in the 10 mM regime.

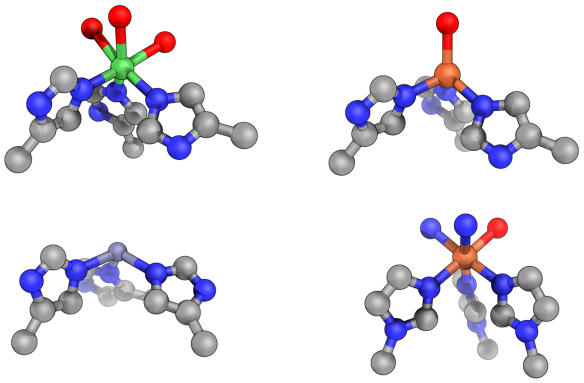

Figure 3. Simplified primary coordination spheres of three-histidine iron enzymes and [**4**]$^+$. Clockwise from top left: PDB 2atf,[27] PDB 2b5h,[28] [**4**]$^+$, PDB 3bal.[29] Color scheme: grey = C; blue = N; red = O; orange = Fe; green = Ni; blue-grey = Zn.

Structural Comparison to Enzymes. In mononuclear Fe(II) three-histidine enzymes, the protein derived facial triad nominally occupies the face of a pseudo octahedron. Likewise, **Tbim** occupies the same face and thereby provide a biomimetic binding mode (Figure 3). However, there are some notable differences. The average benzimidazole Fe–N distance of [**4**]$^+$ is 2.15 Å (average distance for all Fe-N/O bonds in [**4**]$^+$ is 2.16 Å), whereas the average Fe–N/O distance in resting state mammalian cysteine dioxygenase (CDO) determined through K-edge EXAFS is 2.04 Å.[30] Additionally, the protein structures' N–M–N angles are about 100° (average angle 95.7° for 2atf, 100.6° for 2b5h, and 102.4° for 3bal), whereas [**4**]$^+$ has an average N–Fe–N angle of 89.9° for the benzimidazole nitrogen atoms. Also, it is to be noted that, unlike the binding mode in **Tbim** and other synthetic ligands (e.g., **Tp**), the protein active site imidazoles twist into a paddle wheel conformation.

Catalysis. The ability of the **Tbim** system to perform catalytic oxidation was tested using the substrate lithium diethyl 2-phenylmalonate (Li[Phmal]) in accordance with following Limberg's reported biomimetic catalyst (Scheme 4).[17] [Phmal]$^-$ anion is often used as a model substrate instead of acetylacetonate (acac) because acac,[17,31] which is a natural substrate for acetylacetone dioxygenase (Dke1), is difficult to oxidize and sluggish even in nature (k_{cat} = 6.5 s^{-1}).[32] The expected biomimetic product ethyl benzoylformate was independently synthesized and characterized using ^{1}H NMR, ^{13}C NMR, and GC-MS (Figure S20-S22). As a positive control, we attempted to reproduce Limberg's catalytic oxidation of Li[Phmal] wherein they successfully isolated ethyl benzoylformate as the sole product with a TOF of 55 h^{-1} (TON not reported).[17] Unfortunately, our efforts to reproduce this chemistry using [**Tp***Fe(Phmal)] have failed. Specifically, we obtained diethyl 2-hydroxy-2-phenylmalonate (HOPhmal) as the major product following the literature method (Table 1).[17]

Scheme 4. Catalytic 1,3-Diester Oxidation Studies

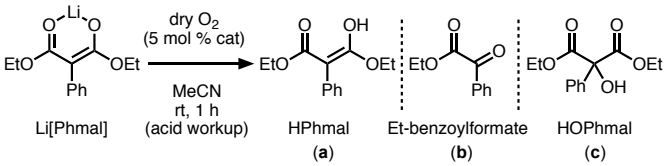

Table 1. Results from catalytic aerobic oxidation of lithium diethyl 2-phenylmalonate (Li[Phmal]).[a]

cat[b]	**a** (%)	**b** (%)	c (%)
Fe/**Tbim** (3:2); "[**4**]$^+$"	0	22	41
Fe/**Tbim** (1:4); "[**3**]$^{2+}$"	0	17	51
[{**Tp***}Fe(Phmal)]	0	21	45
Fe	0	16	41
Fe + Ph$_2$NH	61	0	17
no iron or ligand	77	0	4

[a] Conditions: Substrate added dropwise, 5 mol % catalyst, dry O_2, 1 h; data reported average of two runs, see SI for full data. [b] **Fe** = Fe(OTf)$_2$•2MeCN; **Fe**/**L** represents that complex was prepared *in situ*. If water is not rigorously excluded, HOPhmal (**a**) is the sole product.

Nearly identical results were obtained when [Phmal]$^-$ oxidations were repeated using [**4**]$^+$, [**3**]$^{2+}$, and Fe(OTf)$_2$ (Table 1). In the absence of catalyst, or if water was not rigorously excluded, the HPhmal or HOPhmal was obtained as the major product. These results are actually consistent with another literature report that used electrochemically generated superoxide to oxidize the same lithiated substrate to form ethyl benzoylformate and 2-hydroxy-2-phenylmalonate.[33] Given that the control reaction with iron triflate gives nearly identical results, we conclude that the observed oxidized products arise from superoxide generation by an iron(II) species followed by simple radical-chain oxidation. This is also consistent with Comba's assertion that radical pathways are likely

the general case.[34] We performed a control oxidation with iron triflate and five equiv. diphenylamine, the oxygen radical scavenger, and found that HPhmal was obtained as the major product accompanied by a small amount of HOPhmal. This is strikingly different from the results obtained with iron triflate in the absence of the radical scavenger further indicating that the observed chemistry with all four iron complexes (i.e., $[\mathbf{4}]^{+}$, $[\mathbf{3}]^{2+}$, [{**Tp***}Fe(Phmal)], and $Fe(OTf)_2$) is similar to the known system that relies on electrochemically generated free superoxide.[3334]

Scheme 5. Catalytic Thiolate Oxidation Studies

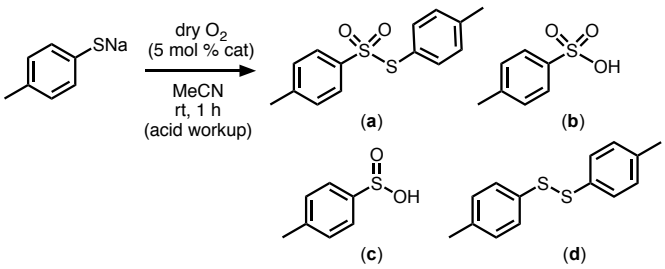

Table 2. Results from catalytic aerobic oxidation of thiocresolate.[a]

cat[b]	**a** (%)	**b** (%)	**c** (%)	**d** (%)
Fe/**Tbim** (3:2); "$[\mathbf{4}]^{+}$"	16	0	54	29
Fe/**Tbim** (1:4); "$[\mathbf{3}]^{2+}$"	5	10	66	18
Fe/**Tp***	9	2	70	19
Fe	15	5	61	19
no iron or ligand (w/o Na_2EDTA)	4	19	71	5
no iron or ligand (w/ Na_2EDTA)	1	6	87	6

[a] Conditions: 5 mol % catalyst, dry O_2, 1 h; data presented average of two runs, see SI for full data. [b] **Fe** = $Fe(OTf)_2$•2MeCN; **Fe**/**L** represents that complex was prepared *in situ*.

Another common substrate used in 3-His biomimetic studies is thiophenolate as a mimic for CDO, which oxidizes aliphatic thiols to sulfinic acids. For instance, the 3-His model ligand **Tpym** was used to model enzyme function by selective oxidation of sodium thiophenolate to phenylsulfinyl acid.[5] In our study, we chose to use sodium thiocresolate because the products are easily examined using ^{1}H NMR spectroscopy; the use of NMR spectroscopy alleviates certain issues that arise from product instability[35] and limitations associated with chromatographic analysis of highly acidic thiophenol oxidation products. Oxidation of thiocresol in MeCN using *in situ* $[\mathbf{4}]^{+}$, $[\mathbf{3}]^{2+}$, Fe**Tp***, and $Fe(OTf)_2$ resulted in similar complicated ranges of products (Scheme 5, Table 2). It has been noted that trace metal impurities- and/or base-catalyzed thiol oxidations can give a variety of products including sulfinic acid.[36,37]

In conclusion, we have synthesized a ligand and coordination complexes with iron that structurally mimics the 3-His active site in nonheme iron enzymes. We also attempted to demonstrate catalytic oxidation chemistry using the substrates LiPhmal and sodium thiocresolate and the results indicate radical-based oxidations. The radical nature of these oxidations, rather than biomimetic-like function, is generally consistent with critical evaluations from others,[34] known literature reactivity of these substrates,[33,36,37] and industrial aerobic oxidation chemistry.[38] While these substrates are often used in biomimetic studies mimicking Dke1 and CDO, our results demonstrate that they are inadequate to conclusively elucidate functional biomimicry. Therefore, future studies using more robust substrates and solvents should be undertaken, and the inclusion of control experiments is paramount. The importance of judiciously chosen control reactions, which are often absent in biomimetic model studies claiming catalytic function, cannot be understated. The lesson here emphasizes the difficulty in producing a *bona fide* biomimetic synthetic nonheme (di)oxygenase where the enzymes incorporate O-atoms from O_2 into substrate through Fe-based O_2-dervied oxidants.

ASSOCIATED CONTENT

Supporting Information.
The Supporting Information is available free of charge.

AUTHOR INFORMATION

Corresponding Author
DCLacy@Buffalo.edu

ACKNOWLEDGMENT

Financial support was provided by the University at Buffalo (UB). This work was completed using the resources of the Chemistry Instrument Center (CIC) and Center for Computational Research (CCR) at UB.

REFERENCES

1. Bruijnincx, P. C. A.; Van Koten, G.; Gebbink, R. J. M. K. Mononuclear Non-Heme Iron Enzymes with the 2-His-1-Carboxylate Facial Triad: Recent Developments in Enzymology and Modeling Studies. *Chem. Soc. Rev.* **2008**, *37*, 2716–2744.
2. Koehntop, K. D.; Emerson, J. P.; Que, L. The 2-His-1-Carboxylate Facial Triad: A Versatile Platform for Dioxygen Activation by Mononuclear Non-Heme Iron(II) Enzymes. *J. Biol. Inorg. Chem.* **2005**, *10*, 87–93.
3. Buongiorno, D.; Straganz, G. D. Structure and Function of Atypically Coordinated Enzymatic Mononuclear Non-Heme-Fe(II) Centers. *Coord. Chem. Rev.* **2013**, *257*, 541–563.

4. Blakesley, D. W.; Payne, S. C.; Hagen, K. S. Spin-State Variation in Solid State and Solution of Mononuclear Iron (II). *Inorg. Chem.* **2000**, *39*, 1979–1989.
5. Anandababu, K.; Ramasubramanian, R.; Wadepohl, H.; Comba, P.; Britto, N. J.; Jaccob, M.; Mayilmurugan, R. A structural and functional model for the tris-histidine motif in cysteine dioxygenase. *Chem. Eur. J.* **2019**, *25*, 9540-9547.
6. Sallmann, M.; Limberg, C. Utilizing the Trispyrazolyl Borate Ligand for the Mimicking of O2-Activating Mononuclear Nonheme Iron Enzymes. *Acc. Chem. Res.* **2015**, *48*, 2734–2743.
7. Reger, D. L.; Little, C. A.; Rheingold, A. L.; Sommer, R.; Long, G. J. Synthesis, Solid-State Structure, Magnetic Properties and Mössbauer Spectral Studies of {Fe[HC(3,5-Me2Pz)3](H2O)3}(BF4)2. *Inorganica Chim. Acta*, **2001**, *316*, 65–70.
8. Tazelaar, C. G. J.; Slootweg, J. C.; Lammertsma, K. Coordination chemistry of tris (azolyl) phosphines. Coord. Chem. Rev. **2018**, 356, 115–126.
9. Sahu, S.; Goldberg, D. P. Activation of Dioxygen by Iron and Manganese Complexes: A Heme and Nonheme Perspective. *J. Am. Chem. Soc.* **2016**, *138*, 11410–11428.
10. Que, L.; Tolman, W. B. Biologically Inspired Oxidation Catalysis. *Nature* **2008**, *455*, 333–340.
11. Oddon, F.; Chiba, Y.; Nakazawa, J.; Ohta, T.; Ogura, T.; Hikichi, S. Characterization of Mononuclear Non-heme Iron(III)-Superoxo Complex with a Five-Azole Ligand Set. *Angew. Chem., Int. Ed.,* **2015**, *54*, 7336-7339.
12. Fischer, A. A.; Lindeman S. V.; Fiedler, A. T. A synthetic model of the nonheme iron-superoxo intermediate of cysteine dioxygenase *Chem. Commun.* **2018**, *54*, 11344.
13. Gordon, J. B.; Vilbert, A. C.; DiMucci, I. M.; MacMillan, S. N.; Lancaster, K. M.; Moëmme-Loccoz, P.; Goldberg, D. P. Activation of dioxygen by a mononuclear nonheme iron complex: Sequential peroxo, oxo, and hydroxo intermediates. *J. Am. Chem. Soc.* **2019**, *141*, 17533-17547.
14. Kass, D.; Corona, T.; Warm, K.; Braun-cula, B.; Kuhlmann, U.; Bill, E.; Mebs, S.; Swart, M.; Dau, H.; Haumann, M.; Hildebrandt, P.; Ray, K. Stoichiometric Formation of an Oxoiron(IV) Complex by a Soluble Methane Monooxygenase Type Activation of O2 at an Iron(II)- Cyclam Center. *J. Am. Chem. Soc.* **2020**, *142*, 5924–5928.
15. Chiang, C.W.; Kleepspies, S. T.; Stout, H. D; Meier, K. K.; Li, P.Y.; Bominaar, E. L.; Que, L.; Münk, E.; Lee, W.Z. Characterization of a paramagnetic mononuclear nonheme iron-superoxo complex. *J. Am. Chem. Soc.* **2014**, *136*, 10846.
16. Blakely, M. N.; Dedushko, M. A.; Poon, P. C. Y.; Villar-Acevedo, G.; Kovacs, J. A. Formation of a reactive, alkyl thiolate-ligated FeIII–superoxo intermediate derived from dioxygen. *J. Am. Chem. Soc.* **2019**, *141*, 1867-1870.
17. Siewert, I.; Limberg, C. A. Trispyrazolylborato iron malonato complex as a functional model for the acetylacetone dioxygenase. *Angew. Chem. Int. Ed*., **2008**, 47, 7953–7956.
18. Debobrata, S.; Paine, T. K. Aerobic Alcohol Oxidation and Oxygen Atom Transfer Reactions Catalyzed by a Nonheme Iron(II)– Alpha-Keto Acid Complex. *Chem. Sci.* **2016**, *7*, 5322–5331.
19. Bruijnincx, P. C. A.; Lutz, M.; Spek, A. L.; Hagen, W. R.; Weckhuysen, B. M.; Van Koten, G.; Gebbink, R. J. M. K. Modeling the 2-His-1-Carboxylate Facial Triad: Iron-Catecholato Complexes as Structural and Functional Models of the Extradiol Cleaving Dioxygenases. *J. Am. Chem. Soc*. **2007**, *129*, 2275–2286.
20. Bruijnincx, P. C. A.; Lutz, M.; Spek, A. L.; Van Faassen, E. E.; Weckhuysen, B. M.; Van Koten, G.; Klein Gebbink, R. J. M. Bis(1-Methylimidazol-2-Yl)Propionates and Bis(1-Methylbenzimidazol-2-Yl)- Propionates: A New Family of Biomimetic N,N,O Ligands - Synthesis, Structures and CuII Coordination Complexes. *Eur. J. Inorg. Chem.* **2005**, 4, 779–787.
21. Moser, A.; Range, K.; York, D. M. Accurate Proton Affinity and Gas-Phase Basicity Values for Molecules Important in Biocatalysis. *J. Phys. Chem. B.* **2010**, *114*, 13911–13921.
22. The p*K*a of 1,2-dimethylbenzimidazole was measured as part of this work (see SI).
23. Martínez, C. H. R.; Dardonville, C. Spectroscopy Using 96-Well Microtiter Plates. *ACS Med. Chem. Lett.* **2013**, *4*, 142–145.
24. Lacy, D. C. Applications of the Marcus Cross Relation to Inner Sphere O_2 Reduction: Implications in Small Molecule Activation. *Inorg. Chem. Front.* **2019**, *6*, 2396–2403.
25. Elgafi, S.; Field, L. D.; Messerle, B. A.; Turner, P.; Hambley, T. W. Rhodium Complexes Containing Bidentate Imidazolyl Ligands: Synthesis and Structure. *J. Organomet. Chem.* **1999**, *588*, 69–77.
26. Sahay, I. I.; Ghalsasi, P. S. Synthesis of New 1,2,3-Triazole Linked Benzimidazole Molecules as Anti-Proliferative Agents. *Synth. Commun.* **2017**, *47*, 825–834.
26. J. G. McCoy, L. J. Bailey, E. Bitto, C. A. Bingman, D. J. Aceti, B. G. Fox, G. N. Phillips, Structure and mechanism of mouse cysteine dioxygenase. *Proc. Natl. Acad. Sci. U.S.A.* **2006**, *103*, 3084-3089.
28. C. R. Simmons, Q. Huang, Q Hao, T. P. Begley, P. A. Karplus, M. H. Stipanuk. Crystal structure of mammalian cysteine dioxygenase. A novel mononuclear iron center for cysteine thiol oxidation. *J. Biol. Chem.* **2006**, *281*, 18723-18733.
29. G. R. Stranzl, U. G. Wagner, G. Straganz, W. Steiner and C. Kratky, Protein Data Bank in Europe, https://www.ebi.ac.uk/pdbe/entry/pdb/3bal, (accessed June 2020), unpublished work.
30. Chai, S. C.; Bruyere, J. R.; Maroney, M. J. Probes of the Catalytic Site of Cysteine Dioxygenase. *J. Biol. Chem.* **2006**, *281*, 15774–15779.
31. (a) Allpress, C. J.; Grubel, K.; Szajna-Fuller, E.; Arif, A. M.; Berreau, L. M. Regioselective aliphatic carbon−carbon bond cleavage by a model system of relevance to iron-containing acireductone dioxygenase. *J. Am. Chem. Soc.* **2013**, *135*, 659-668. (b) Park, H.; Bittner, M. M.; Baus, J. S.; Lindeman, S. V.; Fiedler, A. T. Fe(II) complexes that mimic the active site structure of acetylacetone dioxygenase: O2 and NO reactivity. *Inorg. Chem.* **2013**, *135*, 659-668. (c) Park, H.; Baus, J. S.; Lindeman, S. V.; Fiedler, A. T. Synthesis and characterization of Fe(II) β-diketonato complexes with relevance to acetylacetone dioxygenase: insights into the electronic properties of the 3-histidine facial triad. *Inorg. Chem.* **2011**, *50*, 11978-11989. (d) Ramasubramanian, R.; Anandababu, K.; Kumar, M.; Mayilmurugan, R. Nickel(II) complexes of a 3N ligand as a model for diketon cleaving unusual nickel(II)-dioxygenase enzymes. *Dalton Tran.* **2018**, *47*, 4049-4053.
32. Straganz, G. D.; Nidetzky, B. Reaction coordinate analysis for beta-diketon cleavage by the non-heme Fe2+-dependent dioxygenase Dke1. *J. Am. Chem. Soc.* **2005**, *127*, 12306-12314.
33. Allen, P. M.; Hess, U.; Foote, C. S.; Baizer, M. M.; Electrogenerated bases IV. Reaction of electrogenerated superoxide with some carbon acids. *Synthetic Communications* **1982**, *12*, 123-129.
34. Comba, P.; Lee, Y.M.; Nam, W.; Waleska, A. Catalytic oxidation of alkanes by iron bispidine complexes and dioxygen: oxygen activation *versus* autoxidation. *Chem. Commun.* **2014**, *50*, 412.
35. (a) Kice, J. L.; Bowers K. W. Mechanism of disproportionation of sulfinic acids. *J. Am. Chem. Soc.*, **1962**, *84*, 605 (b) Kice, J. L.; Bowers, K. W. Mechanisms of reactions of sulfinic acids. II. The reaction of *p*-tolyl disulphide with *p*-tolylsulfinic acid. *J. Am. Chem. Soc.* **1962**, *84*, 2384.

36. Bagiyan, G. A.; Koroleva, I. K.; Soroka, N. V.; Ufimtsev, A. V. Oxidation of Thiol Compounds by Molecular Oxygen in Aqueous Solutions. *Russ. Chem. Bull.* **2003**, *52*, 1135–1141.
37. Wallace, T. J.; Schriesheim, A. The base-catalysed oxidation of aliphatic and aromatic thiols and disulfides to sulphonic acids. *Tetrahedron*. **1965**, *21*, 2271-2280.
38. Teles, J. H.; Hermans, I.; Franz, G.; Sheldon, R. A. Ullmann's Encyclopedia of Industrial Chemistry, Wiley-VCH Verlag GmbH & Co. KGaA, 2015, DOI: 10.1002/14356007. a18_261.pub2.

TOC Graphic

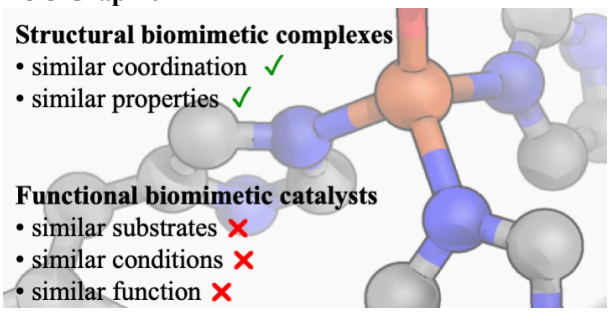
Structural biomimetic complexes
• similar coordination ✓
• similar properties ✓
Functional biomimetic catalysts
• similar substrates ✗
• similar conditions ✗
• similar function ✗

A Facially Coordinating Tris-Benzimidazole Ligand for Nonheme Iron Enzyme Models: Biomimetic or Radical Aerobic Oxidation?

Parami S. Gunasekera,[†] Preshit C. Abhyankar,[†] Samantha N. MacMillan,[§] David C. Lacy*[†]

[†] *Department of Chemistry, University at Buffalo, State University of New York, Buffalo, New York 14260, United States.*
§ *Department of Chemistry and Chemical Biology, Cornell University, Ithaca, New York 14853, United States*

E-mail: DCLacy@buffalo.edu

Contents	**Page**

EXPERIMENTAL

General considerations

All chemicals were used as purchased from chemical vendors unless otherwise noted. Manipulations of air sensitive compounds were carried out in a nitrogen filled Genesis VAC glovebox or using Schlenk techniques to ensure dry and oxygen-free conditions. Dry, oxygen-free solvents were obtained from a PPT solvent purification system and were purified and stored over 3 Å molecular sieves. The acetonitrile used for catalysis was further dried by passing through alumina and stored over 3 Å molecular sieves. The sieves were activated at 200 °C under vacuum for 48 hours prior to use. NMR experiments were carried out on Varian Mercury 300 MHz or Inova 400 MHz spectrometers. ATR-FTIR spectra were collected using a Bruker Alpha IR spectrometer with the "ATR Platinum" insert adapter (diamond crystal), which was stored inside a nitrogen filled VAC Atmospheres glovebox. UV-vis spectra were collected using an 8154 Agilent Spectrophotometer. The pH of the buffer solutions was measured with Mettler Toledo FiveEasy pH meter and a Mettler Toledo glass electrode lE438-IP67 at 25 °C. HRMS was performed using a FT-ICR Brucker 12 T mass spectrometer. GC-MS analysis was performed with a HP 5890 Series II GC containing a J&W Scientific, Inc. column (30 m × 0.250 mm) with a 0.10 µm thin film of phenyl arylene polymer coupled to a HP 5972 Series mass selective detector. Volumetric measurements were carried in analytic grade glassware. All aqueous solutions were prepared using distilled, deionized water. CHN combustion analysis was performed by Robertson Microlit Laboratories, NJ USA. $Fe(OTf)_2$•2MeCN,[1] bis(benzimidazole-2-yl)methane,[2] 2-chloromethyl-1-ethylbenzimidazole,[3] Li[Phmal],[4] ethyl benzoylformate,[5] sodium thiocresol,[6] *p*-toluenesulfinic acid,[7] S-(4-methylphenyl) 4-methylbenzenesulfonothioate[8] and 1,2-di-*p*-tolyldisulfane[9] were prepared according to literature procedures.

Crystallographic methods

Low-temperature X-ray diffraction data for [Fe{**Tbim**}$(MeCN)_2$(OTf)][OTf] (Rlacy28), [Fe{**Tbim**}$(OAc)_2$] (Rlacy31) and [Fe{**Tbim**}$(Cl)_2$] (Rlacy37) were collected on a Rigaku XtaLAB Synergy diffractometer coupled to a Rigaku. Rlacy28 was treated as a racemic twin; the explicit refinement of the Flack parameter yielded a value of 0.450(4). Hypix detector with Cu Kα radiation (λ = 1.54184 Å) from a PhotonJet micro-focus X-ray source at 100 K for Rlacy28 and Rlacy37 and 253 K for Rlacy31. The diffraction images were processed and scaled using the CrysAlisPro software.[10] The structures were solved through intrinsic phasing using SHELXT[11] and refined against F^2 on all data by full-matrix least squares with SHELXL[12] following established refinement strategies.[13] All non-hydrogen atoms were refined anisotropically. All hydrogen atoms were included in the model at geometrically calculated positions and refined using a riding model. The isotropic displacement parameters of all hydrogen atoms were fixed to 1.2 times the U_{eq} value of the atoms they are linked to (1.5 times for methyl groups).

Computational methods

All DFT calculations were performed in ORCA 4.0[14] using the B3LYP functional with atom-pairwise dispersion correction with Becke-Johnson damping[15,16] and def2-SVP[17] basis set. The conductor-like polarizable continuum model (C-PCM) implicit solvation model was used to incorporate solvent effects. All thermochemical calculations were performed at standard conditions (1 atm pressure and 298.15 K). The optimized gas-phase geometries of all molecules were computed and minima were confirmed by the absence of imaginary frequencies. Optimized geometries of MeCN, $[OTf]^-$, $[Fe(MeCN)_4(OTf)_2]$, and the free ligand (**Tbim**) solvated in MeCN were obtained similarly. The single point energies of [Fe(**Tbim**)$(MeCN)_2$(OTf)]$^-$ and [Fe(Tbim)]$^{2+}$ solvated in MeCN were obtained using the cartesian coordinates of the gas-phase optimized molecules. These single point energies were utilized to calculate their solvation Gibb's free enthalpies.

Synthesis

*Synthesis of Bis(1-methylbenzimidazol-2-yl)methane (**2bim**)*: In a glovebox, a 500 mL Schlenk flask equipped with a stir bar was charged with bis(benzimidazole-2-yl)methane (2.73 g, 11.0 mmol) and dissolved in 150 mL of dry DMA. The solution was stirred for 10 minutes. Careful addition of KH (0.972 g, 24.2 mmol) to the solution (CAREFUL: slow addition necessary,) over fifteen minutes caused the solution to turn red and the solution was stirred for an additional 30 minutes after which effervescence ceased. The flask was removed from the glovebox and blanketed with argon on a Schlenk line. Methyl iodide (1.25 mL, 24.6 mmol) was added dropwise to the reaction mixture (by hand with a syringe, ≈3 minutes) and the solution was stirred overnight at room temperature. Open to air, the reaction mixture was poured into 300 mL of rapidly stirring water and the resulting solid was filtered, washed with 50 mL of water and dried under vacuum (2.05 g, 68% yield). ^{1}H NMR data matches with the literature reported values.[2] ^{1}H NMR (Chloroform-*d*, 300 MHz): δ 3.88 (s, 6H, CH_3), 4.67 (s, 2H, CH_2), 7.25 (m, 6H, aromatic), 7.71 (m, 2H, aromatic).

*Synthesis of 2,2'-(2-(1-ethylbenzimidazol-2yl)ethane-1,1-diyl)bis(1-methylbenzimidazole) (**Tbim**)*: In a glovebox, a 100 mL Schlenk tube equipped with a stir bar was charged with **2bim** (0.858 g, 3.11 mmol) to which 20 mL of dry THF was added. The flask was removed from the glovebox and blanketed with argon on a Schlenk line. The solution was cooled to −78 °C, after which *n*-butyllithium (1.37 mL, 3.46 mmol, 2.5 M in hexane) was added to the solution via a syringe and the reaction mixture was stirred for 1 hour (color change from brown to yellow brown). In a glovebox, 2-chloromethyl 1-ethylbenzimidazole (0.587 g, 3.02 mmol) charged in a Schlenk

flask was dissolved in 20 mL of dry THF and stirred for 10 minutes. The solution was taken out of the glovebox and under Schlenk conditions the solution was added dropwise to the reaction mixture containing **2bim** and *n*-butyllithium via cannula transfer. The reaction vessel was left in the cold bath overnight to slowly warm to room temperature with stirring. The reaction mixture was opened to air and quenched with 10 mL of water, volatiles were removed, and the aqueous layer was extracted with ethyl acetate (3 x 30 mL). The organic layer was dried over anhydrous Na_2SO_4 and filtered. The filtrate was evaporated to obtain a yellow orange solid, which was further purified by washing with diethyl either (10 mL) and then hexane (10 mL), and repeating this process two more times. The ligand was obtained as a solid that was purified by column chromatography [ethyl acetate/methanol/ammonium hydroxide (80:19:1)]. Batches varied in color from off white, light pink, to faint yellow (1.14 g, 84% yield). ^{1}H NMR (MeCN-d_3, 300 MHz): δ 1.38 (t, J = 7.2 Hz, 3H, -CH_3), 3.75 (s, 6H, NCH_3), 4.04 (d, J = 7.2 Hz, 2H, -CH_2-), 4.30 (q, J = 7.2 Hz, 2H, NCH_2-), 5.74 (t, J = 7.2 Hz, 1H, -HC meso carbon), 7.17 (dd, J = 13.7, 7.5 Hz, 2H, aromatic), 7.26 (d, J = 7.1 Hz, 1H, aromatic), 7.4 (d, J = 9.2 Hz, 2H, aromatic), 7.54 (dt, J = 15.2, 7.4 Hz, 3H, aromatic). ^{13}C NMR (Chloroform-*d*, 101 MHz): δ 15.13, 30.05, 36.33, 38.37, 109.34, 109.56, 118.97, 119.92, 122.22, 122.30, 134.71, 136.02, 142.38, 142.55, 151.85, 152.34. mp: 205- 208 °C. ATR-FTIR (cm^{-1}): 3052, 2969, 1614, 1457, 1270, 1006, 803, 749, 736, 556, 415. HRMS (LDI/FT-ICR) m/z: Calcd for [2(**Tbim**)+Na]$^+$ 891.43356; Found. 891.43654, Calcd for [**Tbim**+H]$^+$ 435.22972; Found. 435.23023.

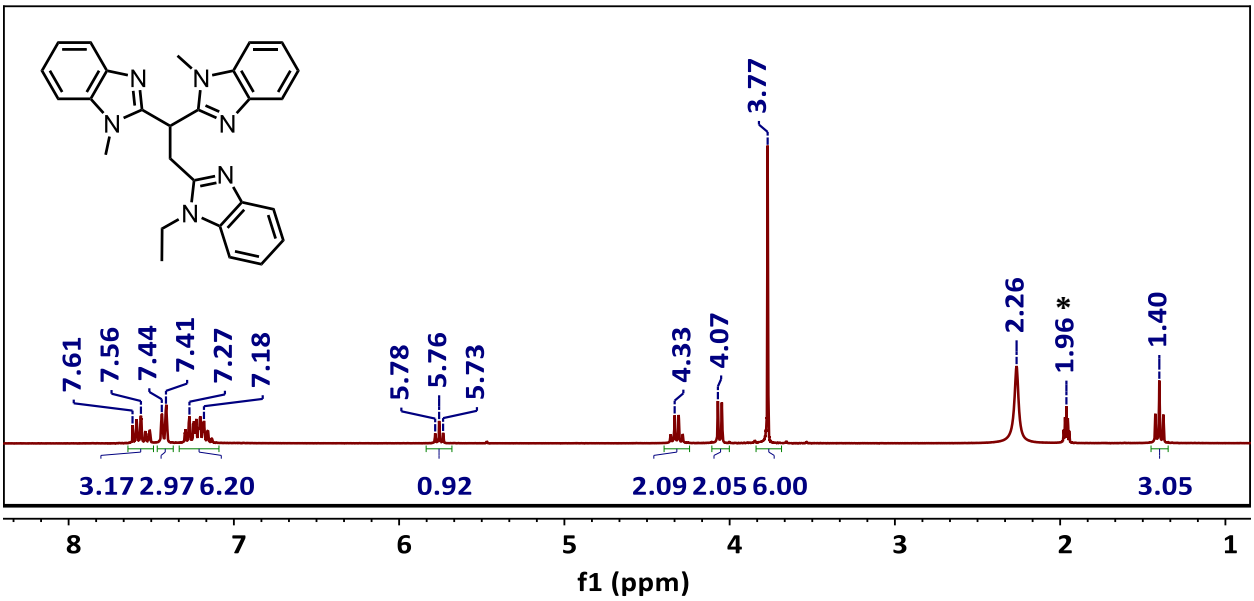

Figure S1: ^{1}H NMR spectrum of **Tbim** in MeCN-d_3*

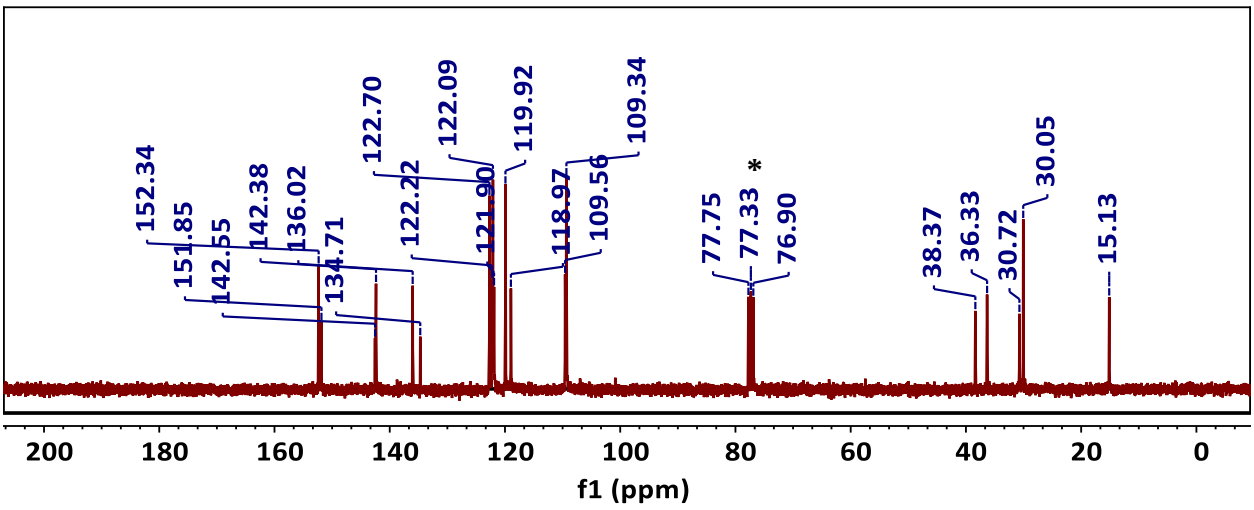

Figure S2: ^{13}C NMR spectrum of **Tbim** in chloroform-*d*

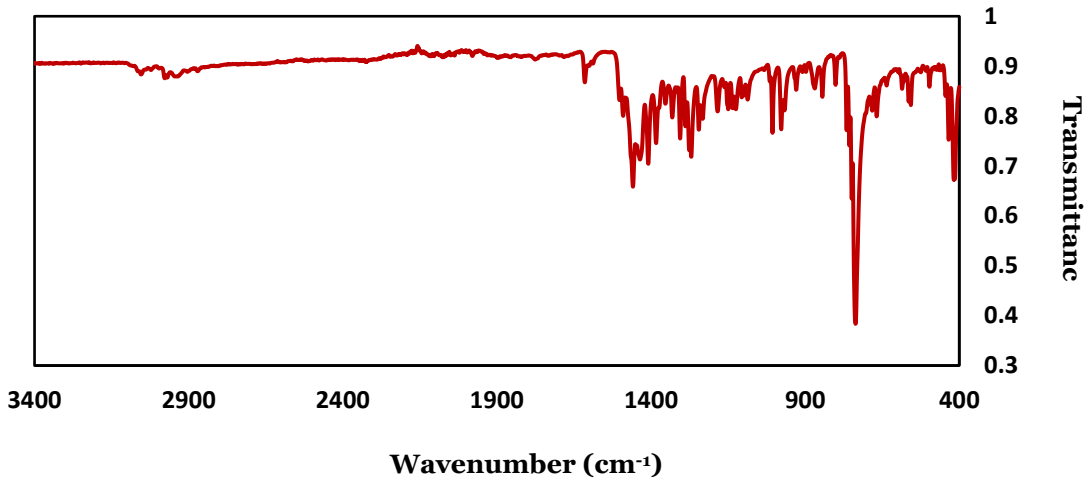

Figure S3: ATR-FTIR spectrum of **Tbim**

Synthesis and characterization of 1, 2, and 3

*[Fe{**Tbim**}(OAc)$_2$] (**1**):* Fe(OAc)$_2$ (40 mg, 0.23 mmol) and **Tbim** (100 mg, 0.230 mmol) was stirred in 15 mL of dry acetonitrile for 1 hour under nitrogen in a glovebox. The solution was removed *in vacuo* and dissolved in 10 mL of dry dichloromethane. Diffusion of diethyl ether into the reaction mixture gave yellow microcrystalline solids (118 mg, isolated yield: 84%). Crystals suitable for XRD were obtained by layering a dichloromethane solution of **1** under diethyl ether. ATR-FTIR (cm^{-1}): 2309, 2279, 1454, 1282, 1236, 1221, 1149, 1028, 748, 634, 1564, 1483, 1409, 1336, 1007, 734, 673. UV-vis (DCM, [ε M^{-1}cm $^{-1}$]): λ_{max} = 209 nm (944). ^{1}H NMR (MeCN-d_3, 300 MHz): δ −20.02, −0.59, −0.20, 1.59, 3.60, 3.93, 4.20, 4.68, 5.62, 5.86, 6.93, 7.20, 7.36, 7.58, 7.77, 8.76, 21.48, 21.77, 88.30. Anal. Calcd (found) for **1**•0.5CH_2Cl_2 ($C_{31.5}H_{32}ClFeN_6O_4$): C, 58.12 (58.36); H, 5.11 (5.16); N, 12.91 (13.05). Evans' method (MeCN-d_3, 300 MHz, 298 K) μ_{eff} =5.31μ_B.

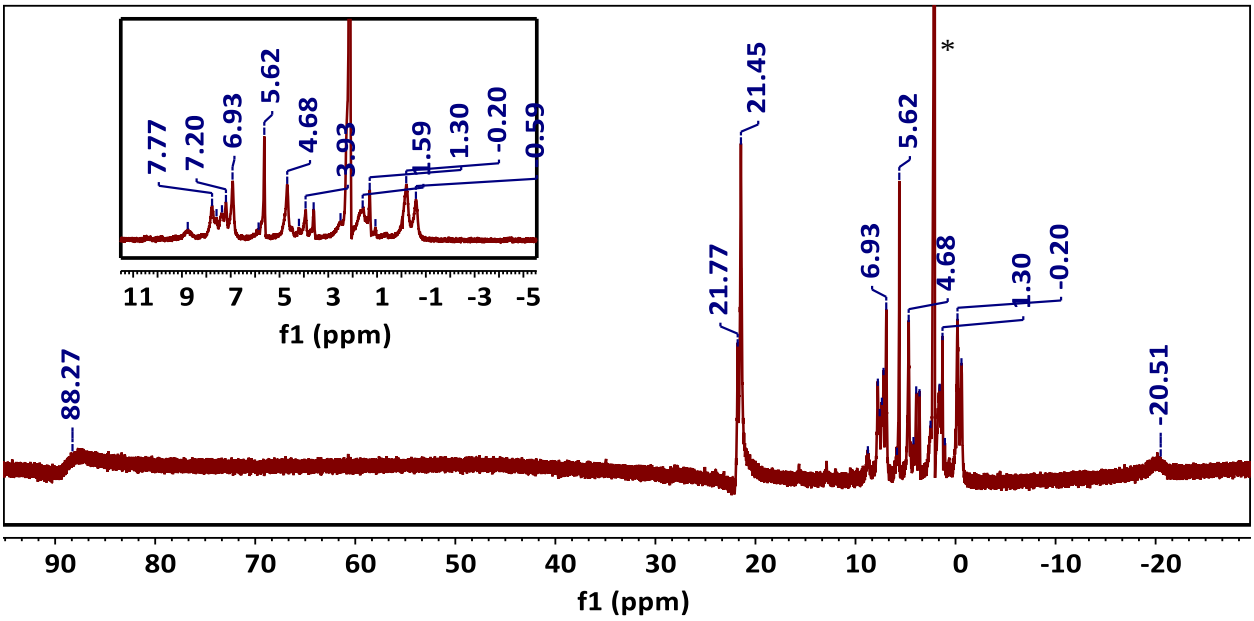

Figure S4: ^{1}H NMR spectrum of **1** in MeCN-d_3*

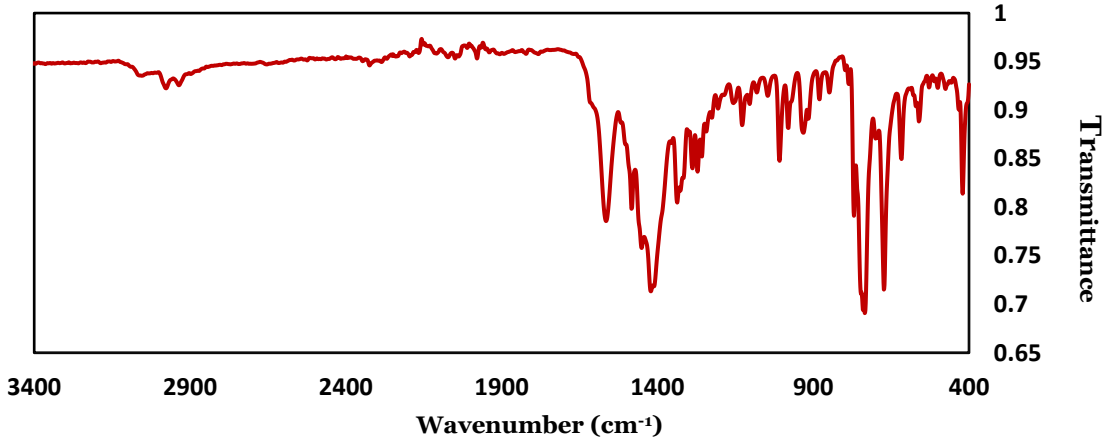

Figure S5: ATR-FTIR spectrum of **1**

*[Fe{**Tbim**}(Cl)$_2$] (**2**):* Anhydrous $FeCl_2$ (12 mg, 0.092 mmol) and **Tbim** (40 mg, 0.092 mmol) were stirred together in 5 mL of dry acetonitrile in a nitrogen filled glovebox. The suspension was treated with methanol dropwise until a homogenous solution was obtained. The solution was further stirred for 1 hour and the resulting reaction mixture was filtered. Diffusion of diethyl ether to the reaction mixture produced colorless crystals of **2** (32 mg, 61% yield). ATR-FTIR (cm^{-1}): 3021, 2978, 1616, 1450, 1402, 1332, 1283, 1149, 1009, 739, 560. ^{1}H NMR (MeOH-d_4, 400 MHz): δ −0.54, −0.32, 1.14, 4.61, 5.94, 6.67, 8.13, 8.91, 9.61, 9.74, 10.22, 11.54, 11.75, 12.30,12.75, 23.66, 25.01, 27.50, 28.29. Anal. Calcd (found) for **2**·0.5CH_2Cl_2 ($C_{31.5}H_{32}ClFeN_6O_4$): C, 58.12 (58.36); H, 5.11 (5.16); N, 12.91 (13.05). HRMS (LDI/FT-ICR) m/z: Calcd for [(**2**)-Cl]$^+$ 525.12569; Found 525.12707. Evans' method (MeOH-d_4, 300 MHz, 298 K) μ_{eff} = 5.79 μ_B.

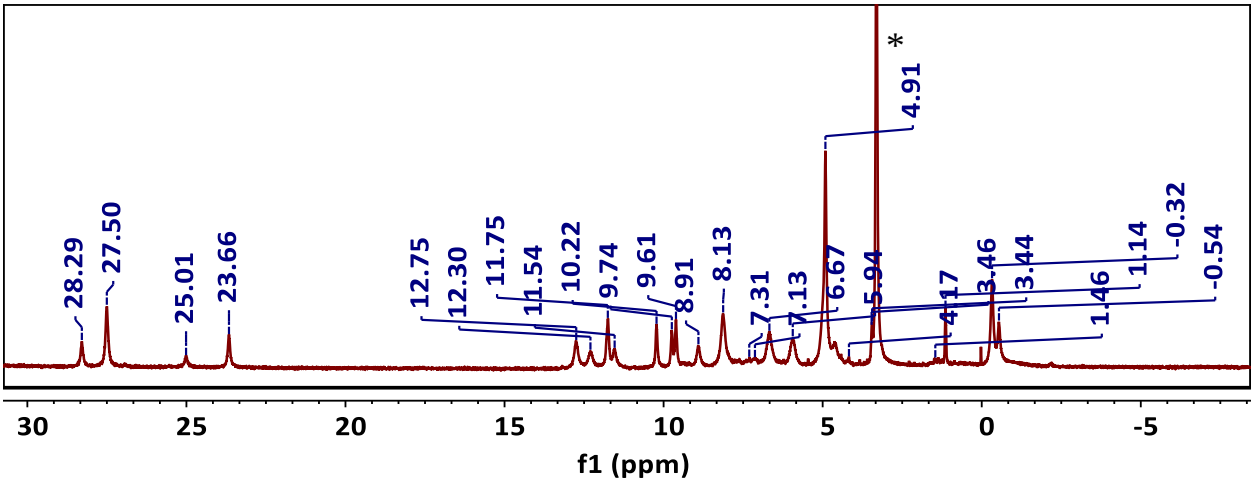

Figure S6: ^{1}H NMR spectrum of **2** in MeOH-d_4*

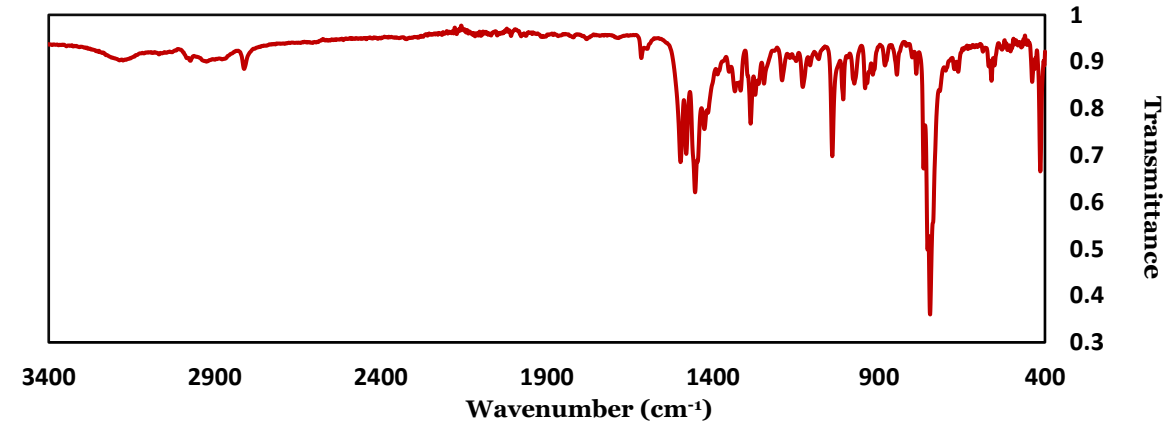

Figure S7: ATR-FTIR spectrum of **2**

*[Fe{**Tbim**}$_2$][BPh$_4$]$_2$ ([**3**][BPh$_4$]$_2$):* Fe(OAc)$_2$ (8 mg, 0.05 mmol) and **Tbim** (20 mg, 0.046 mmol) were mixed together in 1 mL of acetonitrile for 30 minutes. Once the solution became homogenous, the solvent was removed *in vacuo* and the resulting residue was taken up in 5 mL of methanol. The solution was stirred with NaBPh$_4$ (16 mg, 0.046 mmol) and a yellow solid formed that was isolated by filtration and redissolved in a minimum amount of dichloromethane from which crystalline [**3**][BPh$_4$]$_2$ precipitated over 24 hours (18.2 mg, 98% yield). (Figure S16) ATR-FTIR (cm^{-1}): 3052, 2978, 1477, 1448, 1264, 838, 730, 703, 610. ^{1}H NMR (DMSO-d_6, 400 MHz): δ −43.39, −0.51, −0.04, 1.76, 2.07, 2.29, 3.02, 3.59, 3.86, 4.54, 6.26, 6.78, 6.89, 7.15, 7.35, 7.40, 7.66, 8.45, 9.16, 9.81, 11.64, 12.65, 24.12, 24,60, 27.28, 27.74. Evans' method (MeCN-d_3, 300 MHz, 298 K,), μ_{eff} = 5.07 μ_B.

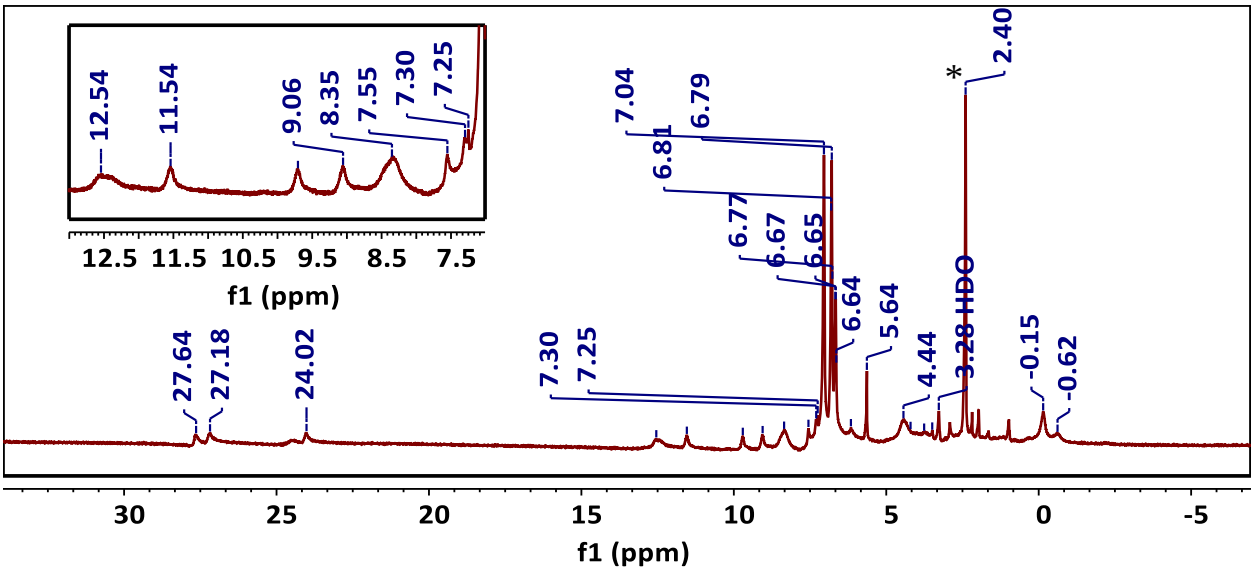

Figure S8: ^{1}H NMR spectrum of [**3**][BPh$_4$]$_2$ in DMSO-d_6*

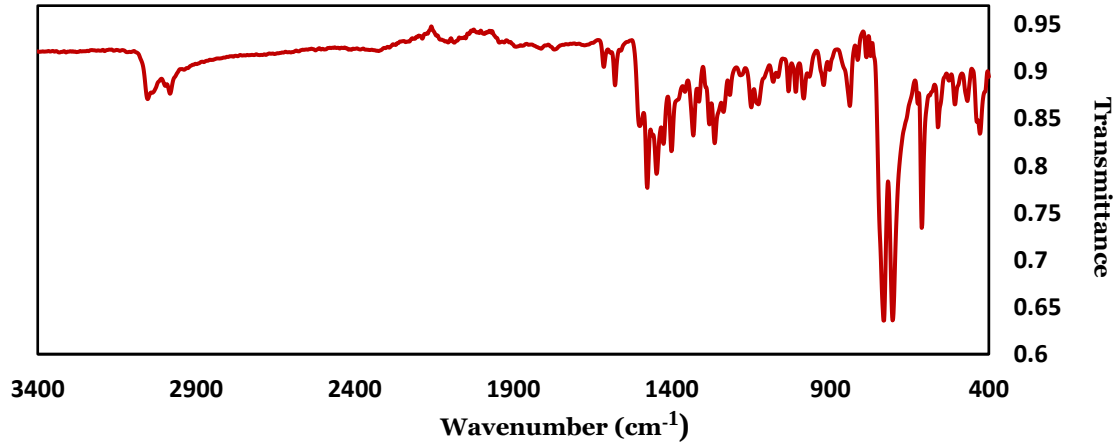

Figure S9: ATR-FTIR spectrum of [**3**][BPh$_4$]$_2$

Preparation of 4

The following procedures are nearly identical, but differ slightly in workup. Isolation of [**4**]$^{+}$ free from [**3**]$^{2+}$ was not accomplished in this work. Synthesis was performed in a nitrogen filled glovebox.

*[Fe{**Tbim**}$_2$][OTf]$_2$ ([**3**][OTf]$_2$):* Fe(OTf)$_2$•2MeCN (24 mg, 0.055 mmol) was stirred in 6 mL of acetonitrile and the ligand **Tbim** (25 mg, 0.055 mmol) and was added to the solution. The reaction was stirred for 1 hour and was filtered. The filtrate was reduced to 1 mL in volume. Crystallization of the acetonitrile reaction mixture by diethyl ether diffusion over 16 hours produced colorless microcrystalline [**3**][OTf]$_2$ (20 mg, 56% yield). Alternatively, the reaction of two equivalents of ligand (30 mg, 0.069 mmol) with one equivalent of the metal salt Fe(OTf)$_2$ (12 mg, 0.035 mmol) in 5 mL of acetonitrile also produced colorless microcrystals of [**3**][OTf]$_2$ (25 mg, 60%). ATR-FTIR (cm^{-1}): 1452, 1405, 1254,1153, 1028, 741, 637. ^{1}H NMR (MeCN-d_3, 300 MHz): δ −45.93, −8.96, −2.10, −0.45, 4.71, 5.05, 5.62, 7.74, 7.97, 8.93, 9.11, 9.63, 10.27, 11.78, 12.49, 12,83, 13.61, 18.68, 23.81, 24.01, 27.05, 27.63, 27.93, 51.74. ^{19}F {^{1}H} NMR (MeCN-d_3, 282.33 MHz): δ −79.76. HRMS (LDI/FT-ICR) m/z: Calcd for {[**3**][OTf]}$^{+}$ 1073.33076; Found 1073.32556. Anal. Calcd (found) for [**3**][OTf]$_2$, $C_{56}H_{52}N_{12}O_6S_2F_6Fe$: C, 54.99 (54.43); H, 4.29 (4.18); N, 13.74 (14.0). Evans' method (MeCN-d_3, 300 MHz, 298 K,), μ_{eff} = 5.06 μ_B.

[*Fe{**Tbim**}(MeCN)$_2$(OTf)][OTf] ([**4**][OTf]):* Fe(OTf)$_2$•2MeCN (36 mg, 0.083 mmol) and **Tbim** (30 mg, 0.069 mmol) was stirred in 4.5 mL of acetonitrile for 1 hour. The resulting solution was pumped off until only trace amounts of acetonitrile remained. The solid/residue was dissolved in 4.5 mL of dichloromethane and was stirred for 1 hour. The solution was filtered to remove unreacted Fe(OTf)$_2$ and [Fe{**Tbim**}$_2$][OTf]$_2$. A drop cast IR of the dichloromethane filtrate indicate the presence of [**4**][OTf] in solution. Diethyl ether diffusion into the reaction filtrate formed colorless crystals of [**4**][OTf] (26 mg, 43% yield) accompanied with microcrystalline [**3**][OTf]$_2$. ATR-FTIR (cm^{-1}): for crystalline [**4**][OTf] 2978, 2931, 2309, 2279, 1657, 1616, 1596, 1454, 1282, 1236, 1221, 1149, 1028, 748, 634. ^{1}H NMR (MeCN-d_3, 400 MHz): δ −8.95, −2.97 −2.10, 3.27, 3.42, 7.72, 8.69, 8.89, 9.70, 11.94, 13.58, 15.84, 18.65, 23.94, 26.67, 26.98, 32.00. ^{19}F {^{1}H} NMR (MeCN-d_3, 282.33 MHz): δ −72.94. CHN and HRMS always contained significant amounts of [**3**]$^{2+}$. HRMS (LDI/FT-ICR) m/z: Calcd for {Fe+**Tbim**+OTf}$^{+}$ 639.10886; Found 639.10884.

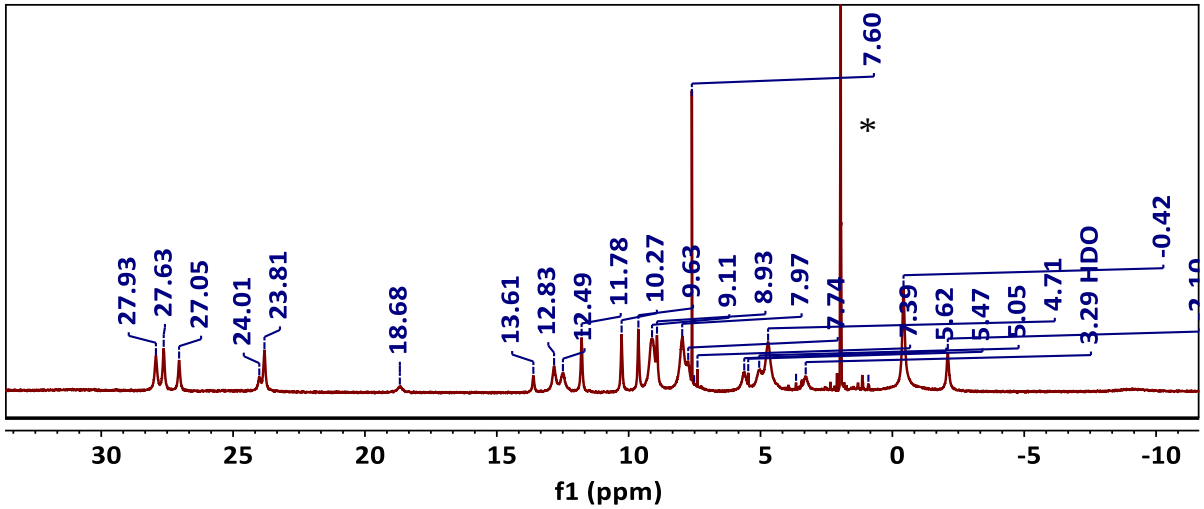

Figure S10: ^{1}H NMR spectrum of [**3**][OTf]$_2$ in MeCN-d_3*

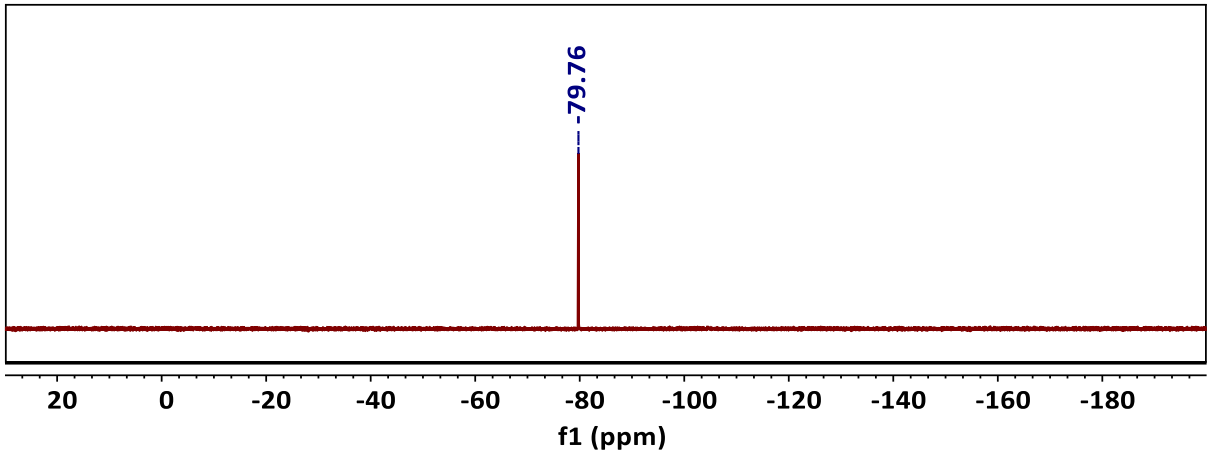

Figure S11: ^{19}F {^{1}H} NMR spectrum of [**3**][OTf]$_2$ in MeCN-d_3

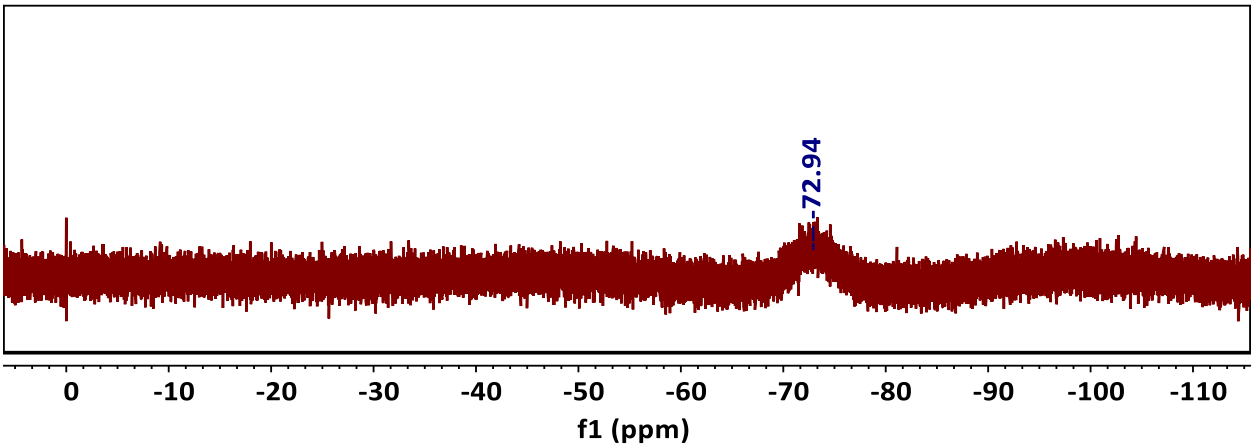

Figure S12: ^{19}F {^{1}H} NMR spectrum of 1:1 mixture of **Tbim** and $Fe(OTf)_2$•2MeCN in MeCN-d_3

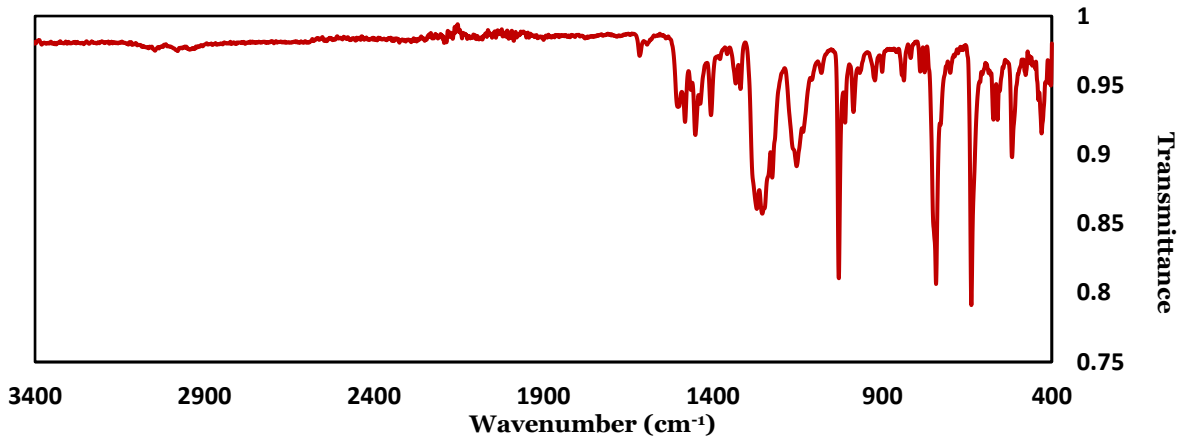

Figure S13: ATR-FTIR spectrum of [**3**][OTf]$_2$

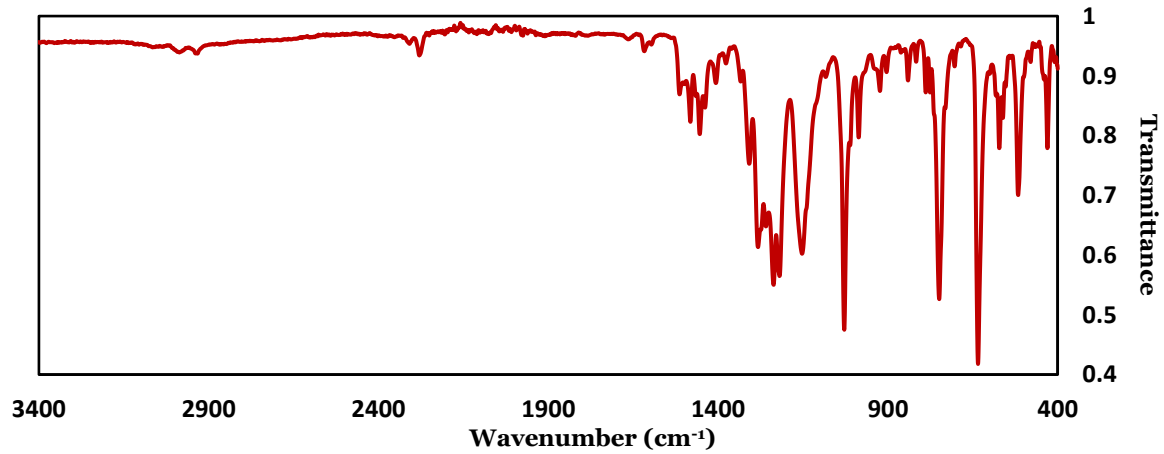

Figure S14: ATR-FTIR spectrum of [**4**][OTf] with MeCN stretches.

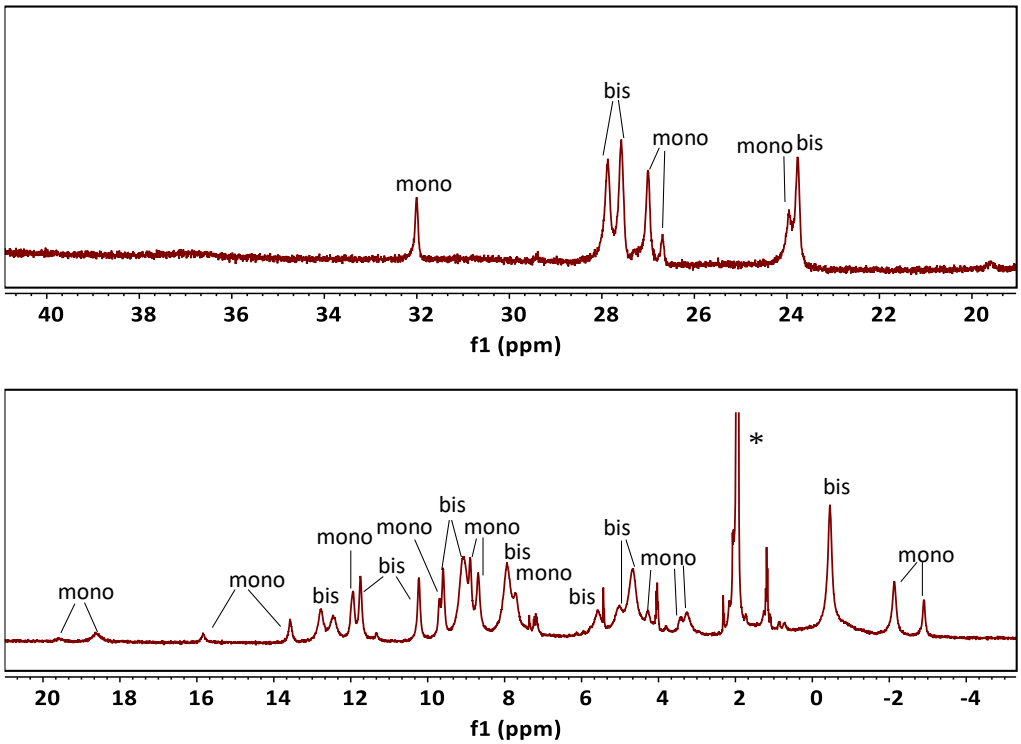

Figure S15: ^{1}H NMR spectrum indicating the presence of [**3**][OTf]$_2$ (bis) and [**4**][OTf] (mono) in MeCN-d_3*

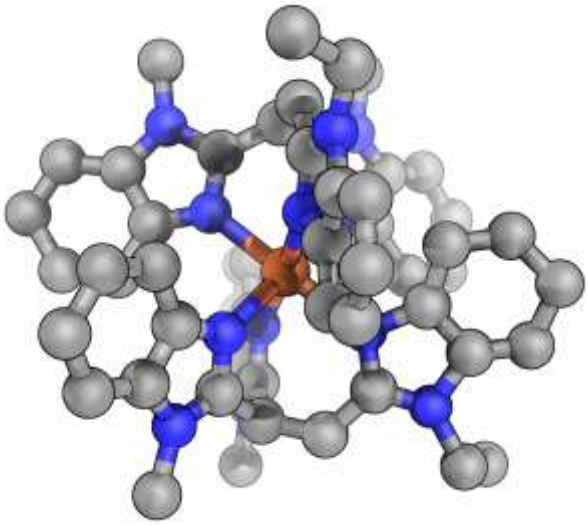

Figures S16: XRD determined connectivity structure of [**3**]$^{2+}$ (crystallized as the tetraphenylborate salt). H-atoms, counterions, and solvent molecules are not shown. Color scheme: orange = Fe; blue = N; grey = C.

Procedure for determining optimal ligand-metal ratio for *in-situ* [4]$^{+}$: Stock solutions of 25 mM **Tbim** and $Fe(OTf)_2$•2MeCN (or $Fe(OTf)_2$•$6H_2O$) were prepared in MeCN-d_3. The stock solutions of the **Tbim** and Fe^{2+} were mixed in different ratios to achieve the desired mole fractions and the total volume was adjusted to 3 mL using MeCN-d_3. The peak at 32 ppm, which was identified as a unique peak for [**4**]$^{+}$, was chosen to construct the plot. The width at half maximum of the 32 ppm peak was measured against the width at half maximum of CH_3 peak of toluene (2.29 ppm, internal standard) or the peak height of acetonitrile (1.94 ppm) in the solution to arrive at a relative intensity value at each mole fraction. The plot was constructed by plotting the relative peak height vs. the mole fraction of **Tbim**/$Fe(OTf)_2$. This measurement was replicated four times, each time with the optimal ratio near 3:2 for metal:ligand.

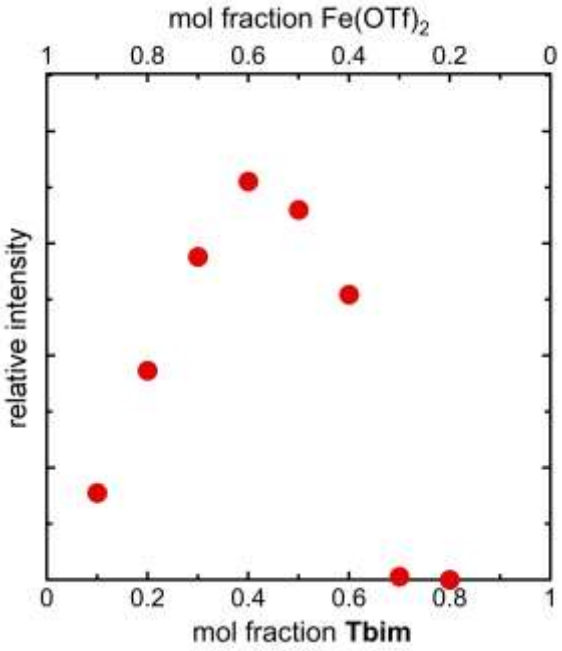

Figure S17: Plot for determining the optimal mole ratio for *in situ* preparation of [**4**]$^{+}$ using $Fe(OTf)_2$•$6H_2O$.

pK_a Measurement

The pK_a (water) values of 1,2-dimethylbenzimidazole were measured with modifications to the procedures reported by Dardonville et. al. and Benkovic et. al.[18,19] Stock solutions of the salts used for buffers were prepared by dissolving the respective salts to get 0.05 M NaH_2PO_4, 0.1 M NaOAc, 0.025 M $Na_2B_4O_7$ and 0.1 M trisodium citrate. 0.1 M HCl was standardized using 0.1 M K_2CO_3 and 0.1 M NaOH was standardized with the HCl solution. The buffer solutions were prepared by measuring 50.0 mL of the appropriate salt solution in a 100.0 mL volumetric flask and adjusting the pH using HCl or NaOH. The ionic strengths of the solutions were calculated using equation 1 and were adjusted to 0.1 M by addition of KCl. The final volume of the buffer solutions was adjusted to 100.0 mL with distilled water.

$$I = \frac{1}{2}\sum_{i=1}^{n} c_i \, z_i \qquad \textit{equation S1}$$

The stock solution of the 1,2-dimethylbenzimidazole was prepared by dissolving of 45 mg of 1,2-dimethylbenzimidazole in 3.0 mL of DMSO. The solutions for the UV-vis experiment was prepared by diluting 20 µL of the stock solution of 1,2-dimethylbenzimidazole to 10.0 mL with the respective buffer solutions. The absorbance spectra of the solution were measured between 200-400 nm and the spectra were normalized to 400 nm. The spectral difference at the lowest pH and each spectrum in different pH was obtained. The wavelengths that produce the highest positive absorbance and the highest negative absorbance were selected. The total absorbance at a given pH was calculated by addition of absolute values of the absorbance at the chosen wavelengths and was plotted against the pH. The pK_a was determined using Origin 2019 by nonlinear regression of equation 2.

$$\textit{Total absorbance} = \frac{[\varepsilon_{HA} - \varepsilon_A][10^{(pH-pK_a)}]}{1+10^{(pH-pK_a)}} \cdot [S_t] \qquad \textit{equation S2}$$

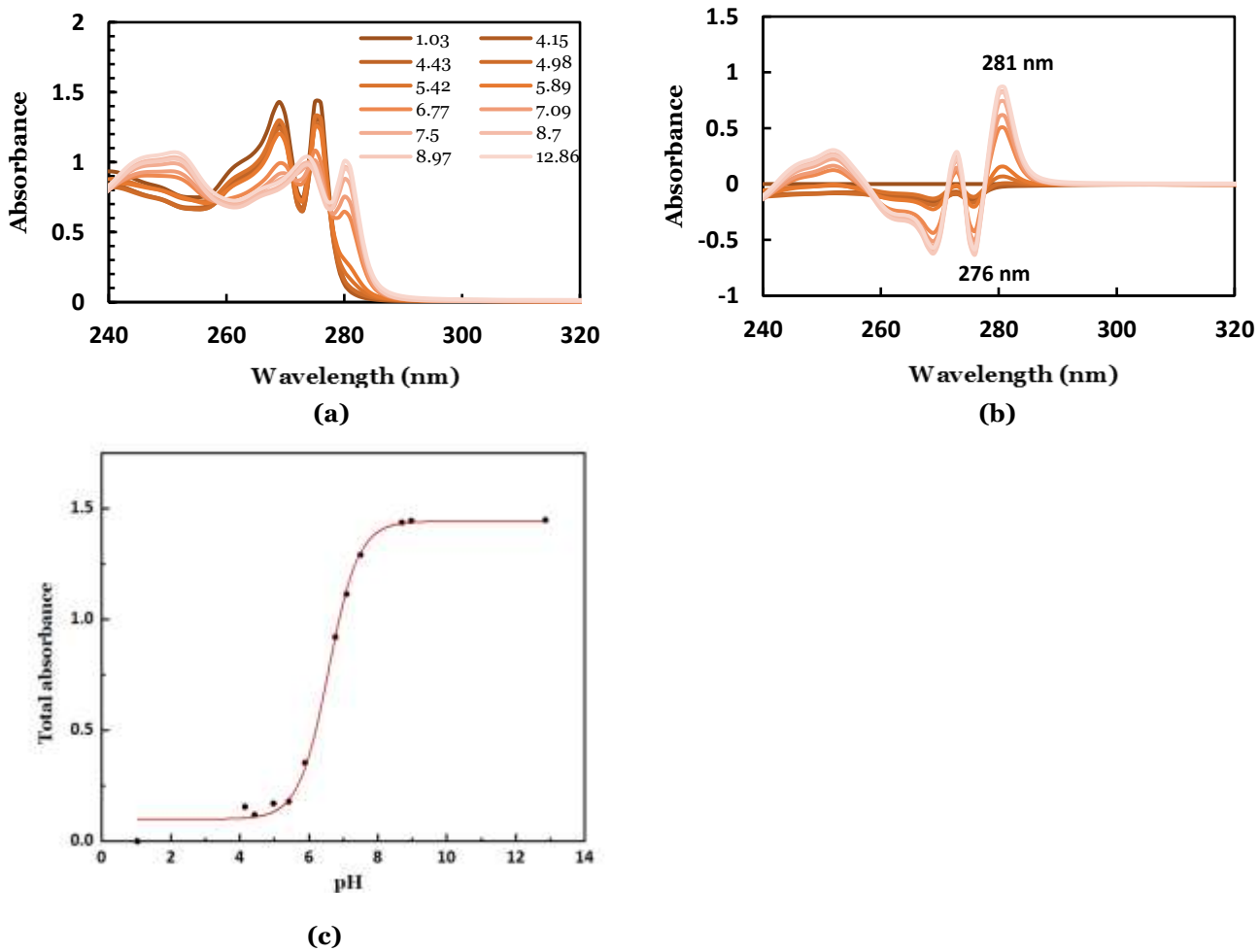

Figure 18: (a) UV-vis spectra of 1,2-dimethylbenzimidazole in different pH buffer solutions (normalized at 400 nm), (b) Plot of the spectral difference between different solutions of 1,2-dimethylbenzimidazole in buffer solutions and (c) Total absorbance difference vs pH graph for determination of pK_a.

Table S1. pK_a (H_2O) values used for Figure 1 and Figure S19.[20]

conjugate acid of…	pK_a	ref
pyrrole	−0.38	21
pyrazole	2.49	21
pyridine	5.23	21,22
benzimidazole	5.43	23
N-methylbenzimidazole	5.55	24
histidine	6.04	21
2-methylbenzimidazole	6.19	21,24
1,2-dimethylbenzimidazole	6.57	this work (see above)
imidazole	6.99	21,25
N-methylimidazole	7.21	25
4-methylimidazole	7.69	25
trimethylamine	9.80	21
H_3TACN	10.44	26
triethylamine	10.75	21
diethylamine	10.84	21
guanidine	13.6	21

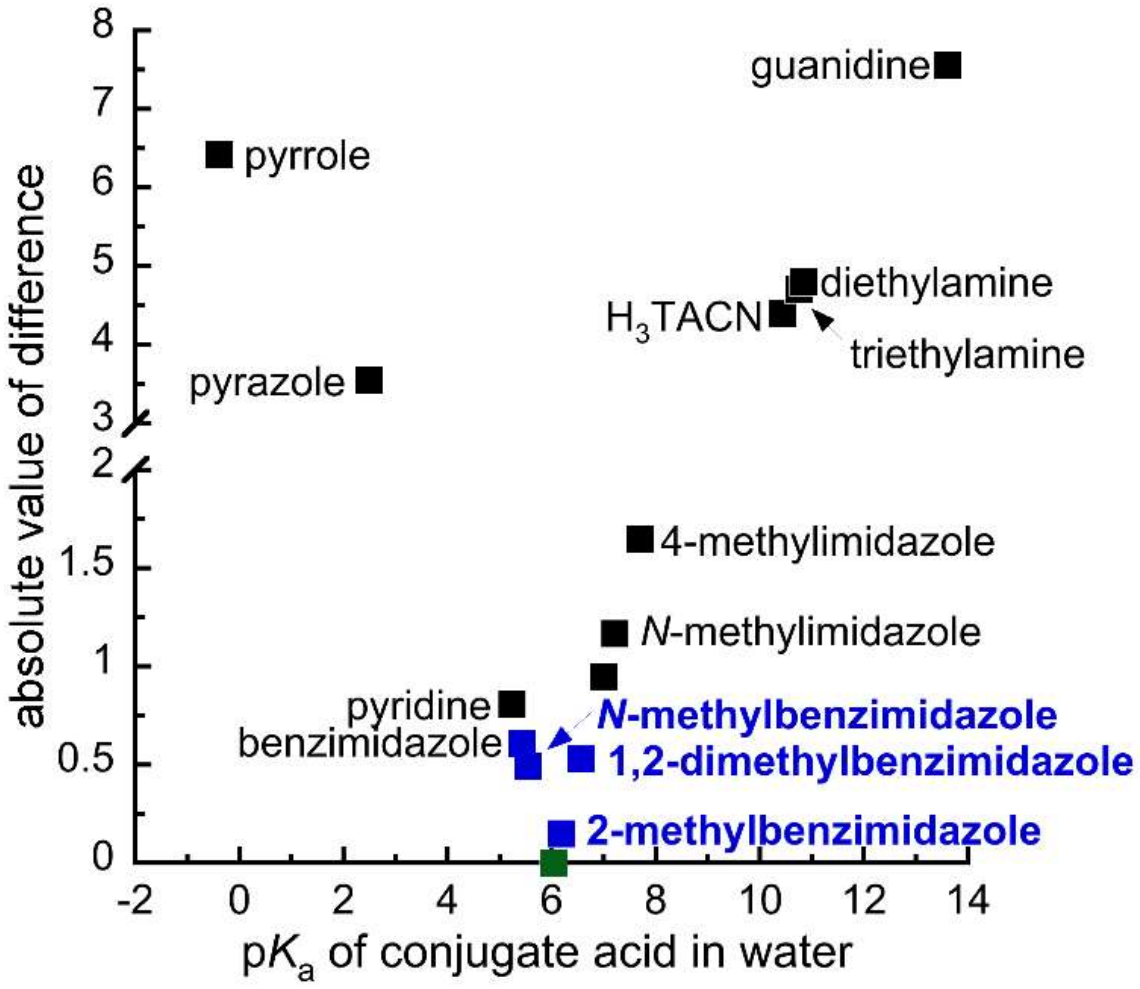

Figure S19: Comparison of ligand conjugate acid pK_a to histidine.

Catalysis

Li[Phmal] oxidation: Following the literature method,[27] dry oxygen was bubbled through a reaction mixture with 5 mol % catalyst in dry acetonitrile over 1 hour and diethyl 2-hydroxy-2-phenylmalonate (HOPhmal) was obtained as the major product; the biomimetic product the ethyl benzoylformate was only a minor product. An increase in ethyl benzoylformate yield was observed for dropwise addition of the substrate with otherwise identical procedures.

The flasks used for catalysis were assembled inside a nitrogen filled glovebox and reactions were performed on a Schlenk line. Stock solutions of **Tbim** (17.8 mg, 0.0410 mmol), [{Tp*}Fe(Phmal)] (24.1 mg, 0.0410 mmol), $Fe(OTf)_2$•2MeCN (67.6 mg, 0.155 mmol) were prepared by dissolving the respective compound in dry acetonitrile and volume was adjusted to 5.0 mL. To produce the catalysts [**4**][OTf] (mono complex) and [**3**][OTf]$_2$ (bis complex) *in situ*, stock solutions of the ligand and the metal were mixed in mole ratios deduced from the plot discussed above (Figure S17) prior to the catalysis. The substrate Li[Phmal] (20.0 mg, 0.0826 mmol) was dissolved in 5 mL of dry acetonitrile and loaded to an addition funnel. The respective catalysts were prepared in 3 mL of dry acetonitrile in a Schlenk flask and stirred for 5 minutes. The setup was taken out from the glovebox and assembled on a Schlenk line. A cannula was inserted for addition of dry oxygen (oxygen was dried by flowing gas through a Drierite column followed by chilled glass tubing, −78 °C). The cannula was submerged and oxygen was bubbled through the solution. Immediately after oxygen bubbling was initiated, substrate was gradually added over a period of 15 minutes *via* a drop funnel. Note that addition of substrate was initiated just before oxygen bubbling. After complete addition of substrate, the funnel was washed with 2 mL of dry acetonitrile and was subsequently added dropwise to the same reaction mixture. Oxygen was bubbled for a total of 1 hour after which 0.5 mL of 3 M HCl was added. The total volume of the solution was adjusted to 10 mL in a volumetric flask with acetonitrile. 200 μL of this solution was treated with a known amount internal standard (anthracene dissolved in DCM) and then diluted to 5 mL with DCM and directly analyzed using GC-MS. Yields were determined using calibration curves prepared from independently synthesized products and reagents with anthracene as the internal standard.

Table S2: Results from catalytic aerobic oxidation of lithium diethyl 2-phenylmalonate (Li[Phmal]) (dropwise addition of substrate).

	HPhmal (%)		Et-benzoylformate (%)		HOPhmal (%)	
Catalyst	run 1	run 2	run 1	run 2	run 1	run 2
Fe/Tbim (3:2)	0	0	18	25	50	31
Fe/Tbim (1:4)	0	0	15	19	61	40
[{Tp*}Fe(Phmal)]	0	0	20	21	47	42
Fe/no ligand	0	0	14	18	42	40
Fe/Ph_2NH	54	68	0	0	13	20
no iron or ligand	88	65	0	0	5	3

Sodium thiocresol oxidation: The flasks used for catalysis were assembled inside a nitrogen filled glovebox and reactions were performed on a Schlenk line. Stock solutions of **Tbim** (29.7 mg, 0.0684 mmol), K[**Tp***] (11.5 mg, 0.0684 mmol), $Fe(OTf)_2$•2MeCN (29.8 mg, 0.0684 mmol) were prepared by dissolving the respective compound in dry acetonitrile and volume adjusted to 5.0 mL. To produce the catalysts [**4**][OTf] (mono complex) and [**3**][$OTf]_2$ (bis complex) *in situ*, stock solutions of the ligand and the metal was mixed in mole ratios deduced from the plot prior to the catalysis. Sodium thiocresol (20.0 mg, 0.137 mmol) was added to the solution of catalyst and charged with a stir bar in a Schlenk flask and total volume was adjusted to 5 mL with dry acetonitrile. The Schlenk flask was taken out of the glovebox and dry oxygen was added to the headspace of the reaction mixture through a cannula (oxygen was dried by flowing gas through Drierite column followed by −78 °C chilled glass tubing). The reaction was stirred for 1 hour with dry oxygen, after which addition of oxygen ceased and the solution was acidified with 1 mL of 3 M HCl to protonate the sodium salts. The solution stirred for another 30 minutes and then the volatiles were removed under vacuum. The residual solid was dissolved in DMSO-d_6 and the yields of the products were determined using ^{1}H NMR spectroscopy. To get a relative conversion, 100% conversion of the substrate was assumed and the yields were calculated using the integration of the methyl peaks (*I*) of the expected products via the following equation.

$$\%\boldsymbol{yield} = \frac{I_{product}}{I_{total}} \times \mathbf{100}\% \qquad \textit{equation S3}$$

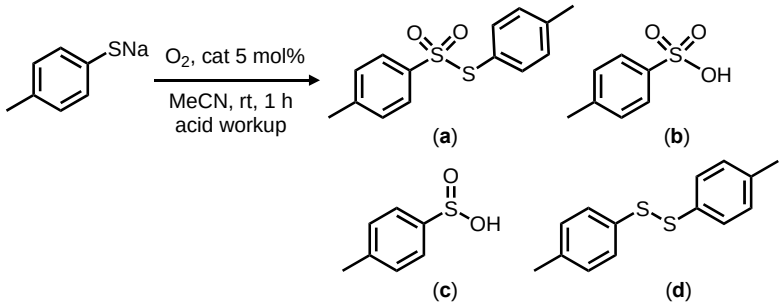

Table S3: Results from catalytic aerobic oxidation of sodium thiocresol.

Catalyst	a (%)		b (%)		c (%)		d (%)	
	run 1	run 2	run 1	run 2	run 1	run 2	run 1	run 2
Fe/Tbim (3:2)	12	21	0	0	53	55	35	24
Fe/Tbim (1:4)	4	6	13	7	63	70	20	16
Fe/Tp*	18	0	5	0	72	67	5	33
Fe/no ligand	12	18	11	0	63	59	15	4
no iron or ligand	5	3	34	5	54	88	6	4

Characterization data for authentic samples

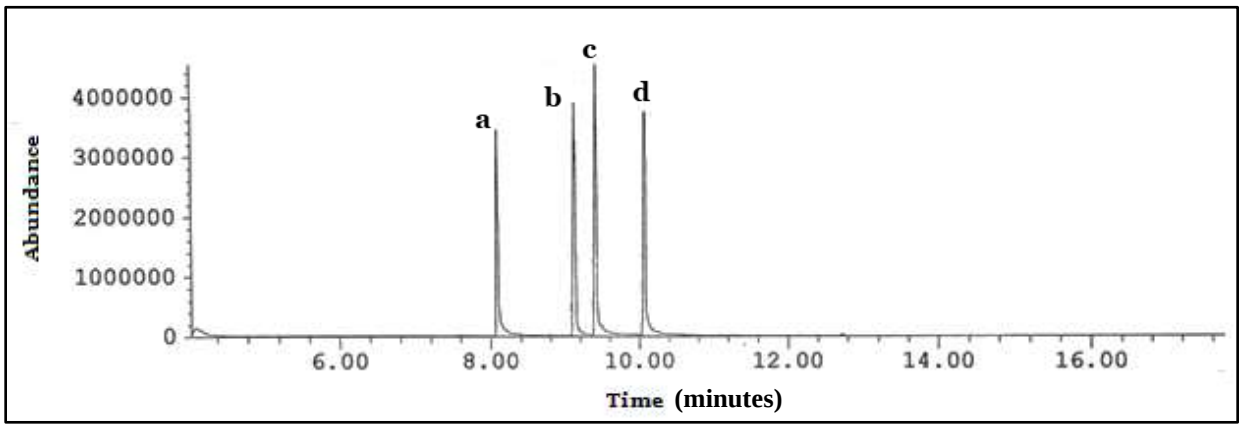

Figure S20: GC trace for HPhmal and its oxidation products prepared independently. **a**: ethyl benzoylformate, **b**: HPhmal, **c**: HOPhmal and **d**: anthracene internal standard.

Ethyl benzoylformate: ^{1}H NMR (Chloroform-*d*, 300 MHz): δ 1.39 (t, 2H), 4.41 (q, 2H), 7.48 (tt, 2H, aromatic), 7.63 (tt, 1H, aromatic), 7.97 (d, 2H, aromatic). ^{13}C NMR (Chloroform-*d,* 75 MHz): δ 14.26, 62.47,129.03, 130.17, 132.63, 135.03, 163.96, 186.56.

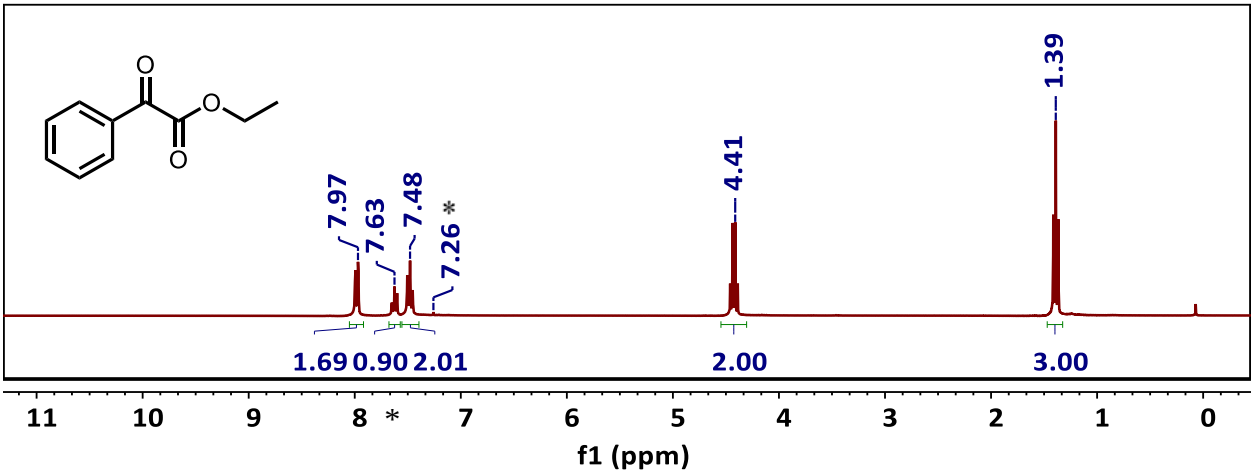

Figure S21: ^{1}H NMR spectrum of ethyl benzoylformate in chloroform-*d*[*]

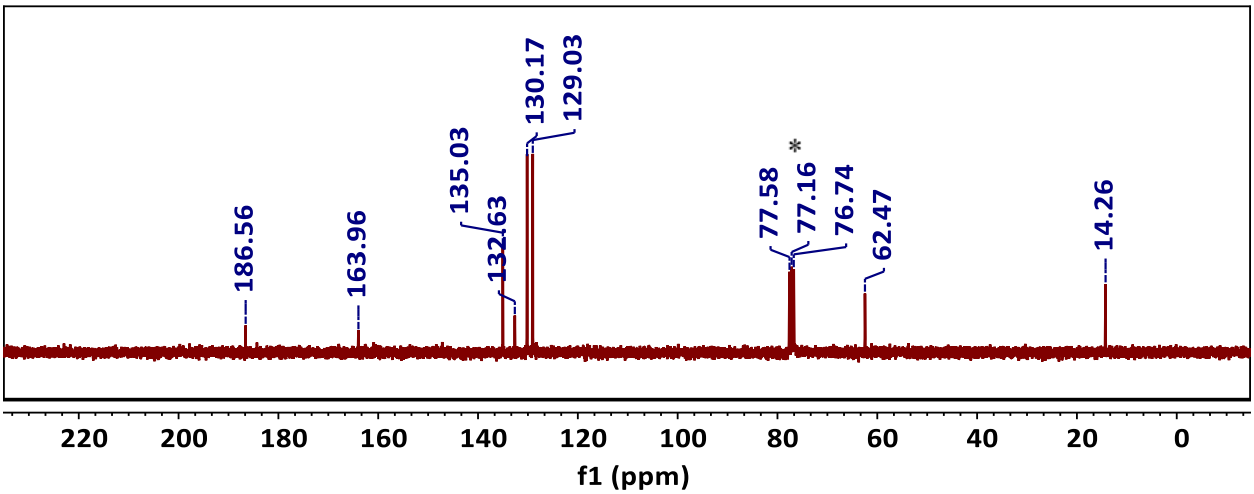

Figure S22: ^{13}C NMR spectrum of ethyl benzoylformate in chloroform-*d*[*]

Diethyl 2-hydroxy-2-phenylmalonate (HOPhmal): Diethyl 2-hydroxy-2-phenylmalonate (HOPhmal) was prepared according to the following procedure: LiPhmal (32 mg, 0.132 mmol) was stirred with 5 mL of dry acetonitrile in the presence of air for 16 hours. The solution was treated with 0.5 mL of 3 M HCl and the solvent was removed under vacuum. The aqueous layer was extracted with 3 x 2 mL of dichloromethane and the solvent evaporated to obtain the product as a colorless clear liquid (23 mg, 70% yield). ^{1}H NMR data matches with the literature reported values.[28] ^{1}H NMR (Chloroform-*d*, 300 MHz): δ 1.28 (t, 6H, CH_3), 4.30 (q, 4H, CH_2), 4.40 (br, 1H, OH), 7.36 (m, 3H, aromatic), 7.65 (d, 2H, aromatic). ^{13}C NMR (Chloroform-*d*, 75 MHz): δ 169.9, 136.0, 128.6, 128.0, 126.7, 80.0, 63.0, 14.0.

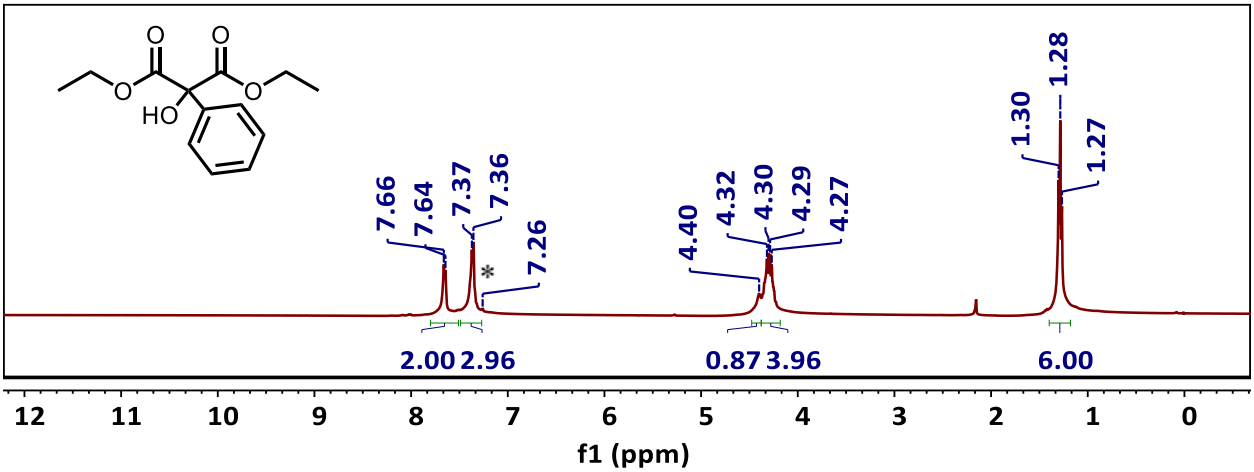

Figure S23: ^{1}H NMR spectrum of HOPhmal in chloroform-*d*[*]

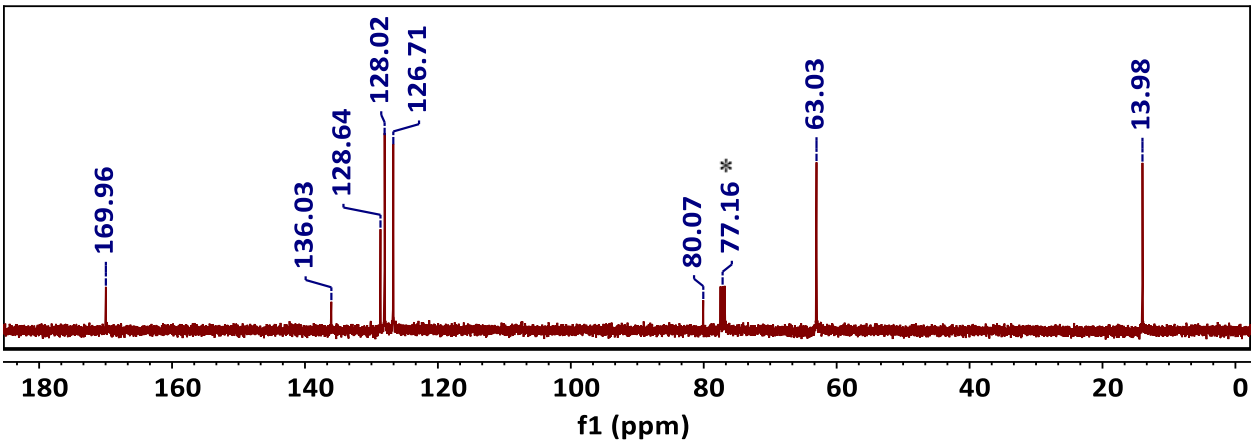

Figure S24: ^{13}C NMR spectrum of HOPhmal in *chloroform-d*[*]

p-toluenesulfinic acid: ^{1}H NMR (*DMSO-d*$_6$, 300 MHz): δ 2.35 (s, 3H), 7.38 (d, 2H, aromatic), 7.54 (d, 2H, aromatic)

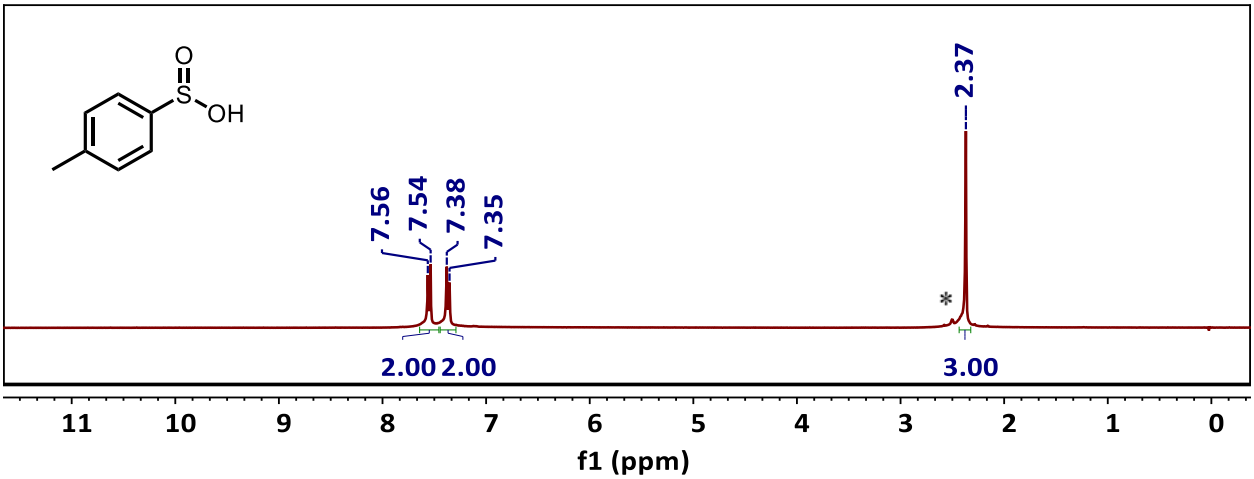

Figure S25: ^{1}H NMR spectrum of *p*-toluenesulfinic acid in DMSO-d_6*

1,2-di-p-tolyldisulfane: ^{1}H NMR (DMSO-d_6, 300 MHz): δ 2.28 (s, 3H), 7.20 (d, 4H, aromatic), 7.38 (d, 4H, aromatic)

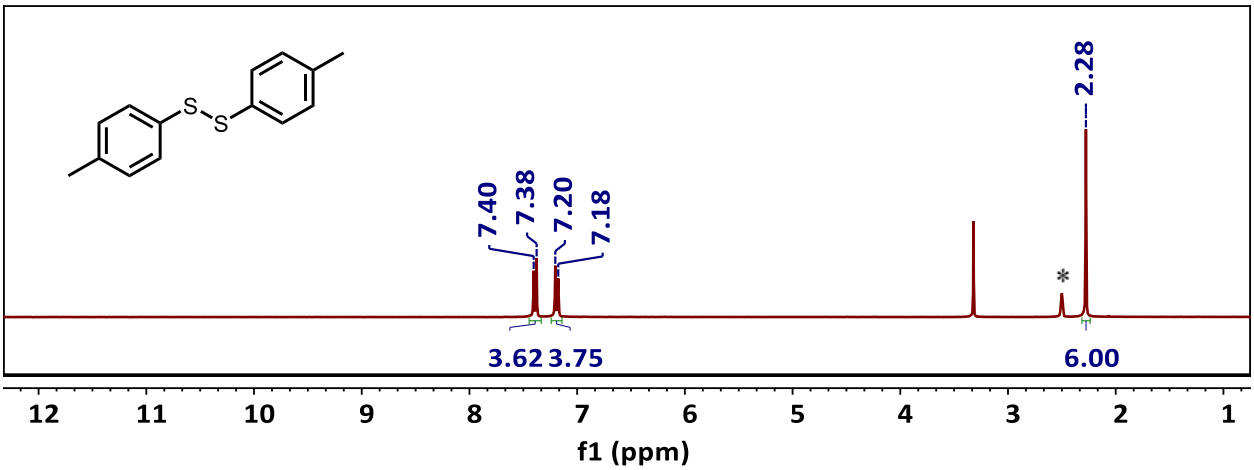

Figure S26: ^{1}H NMR spectrum of 1,2-di-*p*-tolyldisulfane in DMSO-d_6*

p-toluenesulfonic acid: ^{1}H NMR (DMSO-d_6, 300 MHz): δ 2.29 (s, 3H), 7.14 (d, 4H, aromatic), 7.48 (d, 4H, aromatic)

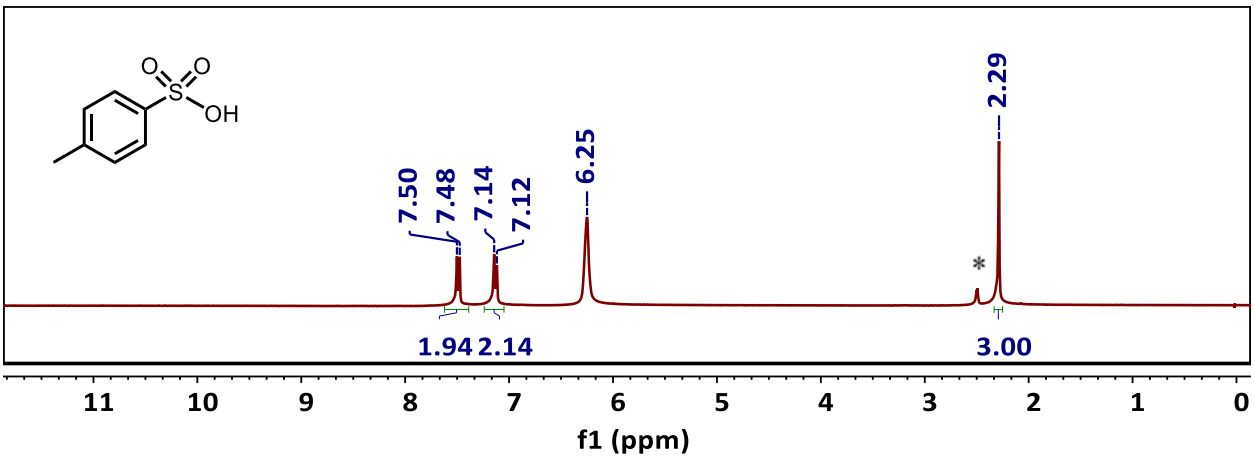

Figure S27: ^{1}H NMR spectrum of *p*-toluenesulfonic acid in DMSO-d_6*

S-(4-methylphenyl) 4-methylbenzenesulfonothioate: ^{1}H NMR (DMSO-d_6, 300 MHz): δ 2.32 (s, 3H), 2.37 (s, 3H), 7.20 (q, 4H, aromatic), 7.41 (q, 4H, aromatic)

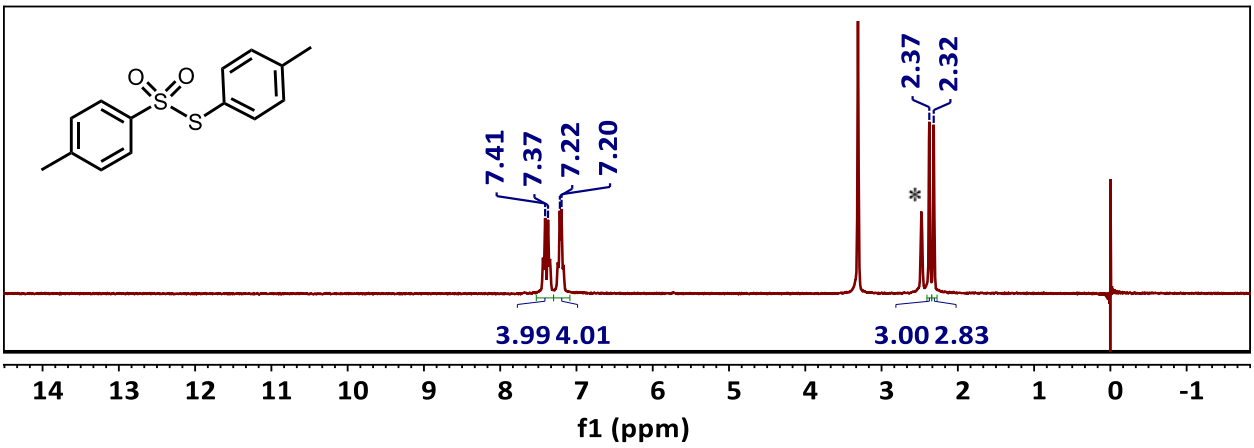

Figure S28: ^{1}H NMR spectrum of S-(4-methylphenyl) 4-methylbenzenesulfonothioate in DMSO-d_6*

Determination of Schlenk equilibrium from DFT: The Gibb's free energy changes at standard conditions in gas phase (ΔG_{gas}) and in MeCN (ΔG_{MeCN}) were calculated for the following reactions;

$$[Fe(\mathbf{Tbim})_2][OTf]_2 + 2\ MeCN \rightleftharpoons [Fe(\mathbf{Tbim})(MeCN)_2(OTf)][OTf] + \mathbf{Tbim} \quad \textit{Rxn. 1}$$

$$[Fe(\mathbf{Tbim})_2][OTf]_2 + \textit{trans}\text{-}[Fe(MeCN)_4(OTf)_2] \rightleftharpoons 2\ [Fe(\mathbf{Tbim})(MeCN)_2(OTf)][OTf] \quad \textit{Rxn. 2}$$

$$\textit{trans}\text{-}[Fe(MeCN)_4(OTf)_2] + \mathbf{Tbim} \rightleftharpoons [Fe(\mathbf{Tbim})(MeCN)_2(OTf)][OTf] + 2\ MeCN \quad \textit{Rxn. 3}$$

$$\textit{trans}\text{-}[Fe(MeCN)_4(OTf)_2] + 2\ \mathbf{Tbim} \rightleftharpoons [Fe(\mathbf{Tbim})_2][OTf]_2 + 4\ MeCN \quad \textit{Rxn. 4}$$

Table 4: DFT computed Gibbs's free energies for Schlenk equilibrium

Reaction	ΔG_{gas} (kcal/mol)	ΔG_{MeCN} (kcal/mol)
Rxn. 1	-96.75	+32.31
Rxn. 2	-41.91	+3.163
Rxn. 3	+54.84	-29.14
Rxn. 4	+151.6	-61.45

References

1. Hagen, K. S. Iron(II) Triflate Salts as Convenient Substitutes for Perchlorate Salts:Crystal Structures of $[Fe(H_2O)_6](CF_3SO_3)_2$ and $Fe(MeCN)_4(CF_3SO_3)_2$. *Inorg. Chem.* **2000**, *39*, 5867–5869.
2. lgafi, S.; Field, L. D.; Messerle, B. A.; Turner, P.; Hambley, T. W. Rhodium Complexes Containing Bidentate Imidazolyl Ligands: Synthesis and Structure. *J. Organomet. Chem.* **1999**, *588*, 69–77.
3. Sahay, I. I.; Ghalsasi, P. S. Synthesis of New 1,2,3-Triazole Linked Benzimidazole Molecules as Anti-Proliferative Agents. *Synth. Commun.* **2017**, *47*, 825–834.
4. Siewert, I.; Limberg, C. A Trispyrazolylborato iron malonato complex as a functional model for the acetylacetone dioxygenase. *Angew. Chem. Int. Ed.* **2008**, 47, 7953–7956.
5. Yamada, T.; Kuwata, M.; Takakura, R.; Monguchi, Y.; Sajiki, H.; Sawama, Y. Organocatalytic Nitroaldol Reaction Associated with Deuterium-Labeling. *Adv. Synth. Catal.* **2018**, *360*, 637–641.
6. Vibert, F.; Marque, S. R. A.; Bloch, E.; Queyroy, S.; Bertrand, M. P.; Gastaldi, S.; Besson, E. Design of Wall-Functionalized Hybrid Silicas Containing Diazene Radical Precursors. EPR Investigation of Their Photolysis and Thermolysis. *J. Phys. Chem. C.* **2015**, *119*, 5434–5439.
7. Reichardt, C.; Erfurt, H. P.; Harms, K.; Schäfer, G. Syntheses, Absolute Configurations, and UV/Vis Spectroscopic Properties of New Chiral Tri- and Pentamethinium Streptocyanine Dyes with 4-Aminophenyl 4-Methylphenyl Sulfoxide Endgroups. *European J. Org. Chem.* **2002**, *3*, 439–452.
8. Zhao, X.; Liu, T. X.; Zhang, G. Synthesis of Thiosulfonates via CuI-Catalyzed Reductive Coupling of Arenesulfonyl Chlorides Using $Na2SO_3$ or $NaHSO_3$ as Reductants. *Asian J. Org. Chem.* **2017**, *6*, 677–681.
9. Kirihara, M.; Asai, Y.; Ogawa, S.; Noguchi, T.; Hatano, A.; Hirai, Y. A Mild and Environmentally Benign Oxidation of Thiols to Disulfides. *Synthesis.* **2007**, *21*, 3286–3289.
10. CrysAlisPro; Rigaku OD, The Woodlands, TX, 2015.
11. Sheldrick, G. M., SHELXT – Integrated Space-Group and Crystal-Structure Determination. Acta Cryst. **2015**, *A71*, 3-8.
12. Sheldrick, G.M. A Short History of SHELX. *Acta Cryst.* **2008**, *A64*, 112-122.
13. Müller, P. Practical Suggestions for Better Crystal Structures. *Crystallogr. Rev.* **2009**, *15*, 57-83.
14. (a) Neese, F. Wiley *Interdiscip. Rev. Comput. Mol. Sci.* **2012**, 2, 73. (b) Neese, F. Wiley *Interdiscip. Rev. Comput. Mol. Sci.* **2018**, *8*, 4.
15. (a) Grimme, S.; Ehrlich, S.; Goerigk, L. J. *Comput. Chem.* **2011**, *32*, 1456. (b) Grimme, S.; Antony, J.; Ehrlich, S.; Krieg, H. *J. Chem. Phys.* **2010**, *132*, 154104.
16. (a) Johnson E. R.; Becke, A. D. *J. Chem. Phys.* **2005**, *123*, 024101. (b) Becke, A. D.; Johnson, E. R. *J. Chem. Phys.* **2005**, *123*, 154101. (c) Johnson, E. R.; Becke, A. D. *J. Chem. Phys.* **2006**, *124*, 174104.
17. Weigend, F.; Ahlrichs, R. *Phys. Chem. Chem. Phys.* **2005**, *7*, 3297.
18. Martínez, C. H. R.; Dardonville, C. Spectroscopy Using 96-Well Microtiter Plates. *ACS Med. Chem. Lett.* **2013**, *4*, 142–145.
19. Tomsho, J. W.; Pal, A.; Hall, D. G.; Benkovic, S. J. Ring Structure and Aromatic Substituent Effects on the pK_a. *ACS Med. Chem. Lett.* **2012**, *3*, 48–52.
20. Moser, A.; Range, K.; York, D. M. Accurate Proton Affinity and Gas-Phase Basicity Values for Molecules Important in Biocatalysis. *J. Phys. Chem. B.* **2010**, *114*, 13911–13921.

21. Haynes, W. M. CRC Handbook of Chemistry and Physics- Dissociation Constants of Organic Acids and Bases, 2010-2011. Josep A. DiVerdi-University of Colorado https://sites.chem.colostate.edu/diverdi/all_courses/CRC%20reference%20data/dissociation%20constants%20of%20organic%20acids%20and%20bases.pdf (accessed on March 5, 2020).
22. Kyrgowski, T. M.; Szatylowicz, H.; Zachara, J. E. How H-bonding Modifies Molecular Structure and π-Electron Delocalization in the Ring of Pyridine/Pyridinium Derivatives Involved in H-Bond Complexation. *J. Org. Chem.* **2005**, *70*, 8859-8865.
23. Walba, H. & Isensee, R. W. Acidity constants of some arylimidazoles and their cations. *J. Org. Chem.* **1961**, *26*, 2789-2791.
24. Jerez, G.; Kaufman, G.; Prystai, M.; Schenkeveld, S.; Donkor, K. K. Determination of thermodynamic pK_a values of benzimidazole and benzimidazole derivatives by capillary electrophoresis. *J. Sep. Sci.* **2009**, *32*, 1087-1095.
25. a) A. H. M. Kirby and A. Neuberger, *Biochem. J.* **1938**, *32*, 1146. (b) Lenarcik., B.; Ojczenasz, P. *J. Heterocyclic Chem.* **2002**, *39*, 287.
26. Neis, C.; Petry, D.; Demangeon, A.; Morgenstern, B.; Kuppert, D.; Huppert, J.; Stucky, S.; Hegetschweiler, K. *Inorg. Chem.* **2010**, *49*, 10092.
27. Siewert, I.; Limberg, C. A. Trispyrazolylborato iron malonato complex as a functional model for the acetylacetone dioxygenase. *Angew. Chem. Int. Ed.*, **2008**, 47, 7953–7956.
28. Miao, C. B.; Wang, Y. H.; Xing, M. L.; Lu, X. W.; Sun, X. Q.; Yang, H. T. I2-Catalyzed Direct α-Hydroxylation of β-Dicarbonyl Compounds with Atmospheric Oxygen under Photoirradiation. *J. Org. Chem.* **2013**, *78*, 11584–11589.